

**THE OCCURRENCE OF CONTRACTION-INDUCED LESIONS IN THE
SARCOLEMMA OF SKELETAL MUSCLES: INSIGHTS FROM A MICRO-
SIZED WHOLE MUSCLE MODEL**

by

Rainer N. Ng

A dissertation submitted in partial fulfillment
of the requirements for the degree of
Doctor of Philosophy
(Biomedical Engineering)
in The University of Michigan
2008

Doctoral Committee:

Professor John A. Faulkner, Chair
Professor Ari Gafni
Associate Professor Susan Brooks Herzog
Assistant Professor Michael Mayer

© Rainer N. Ng

2008

Dedicated to my mother, Theresa, for her utmost courage
To Richard Dawkins and Carl Sagan
who have helped me appreciate the exquisite
sophistication and beauty of life on planet Earth

Acknowledgements

Equipped with his five senses, man explores the universe around him and calls the adventure Science.

-Edwin Powell Hubble, *The Nature of Science*, 1954

I am honored and privileged to have contributed, in a small way, to mankind's understanding of the natural world. This dissertation would not have been possible without the involvement and support of many individuals. I would especially like to thank John Faulkner for his mentorship and trust – giving me the academic freedom to define, develop and pursue a variety of research interests. Gratitude is also extended to my committee members Susan Brooks, Ari Gafni and Michael Mayer who have provided keen insight and advice. Finally, I would like to thank Dennis Claflin for his tremendous patience, help and advice.

TABLE OF CONTENTS

Dedication	ii
Acknowledgements	iii
List of Figures	v
Abstract	vi
Chapters	
1. Introduction	1
2. The benefits of a miniature whole muscle model for studies of prolonged, repetitive contractile activity <i>in vitro</i>	22
3. Poloxamer 188 reduces the contraction-induced force decline in lumbrical muscles from <i>mdx</i> mice	39
4. Fluorescent indicators reveal no evidence of sarcolemmal lesions in whole skeletal muscles during lengthening contractions	61
5. Summary and Conclusion	87

LIST OF FIGURES

Figure		
1.1	Spatial orientation of actin and myosin filaments	10
1.2	The cross bridge cycle	11
2.1	Force production of lumbrical muscles	32
2.2	Visualization of injured muscle fibers with Evans Blue Dye and FM1-43	33
2.3	Measurements of FM1-43 intensity in muscles during isometric and lengthening contraction protocols	34
3.1	Lumbrical muscle from the 3 rd digit of the forepaw of a mouse	52
3.2	Force production of WT and <i>mdx</i> lumbrical muscles	53
3.3	Force production of WT and <i>mdx</i> lumbrical muscles at the end of 20 isometric contractions	54
4.1	Measurements from ratioable indicator Fura-PE3 transform Fluo-4 fluorescence into a pseudo-ratio signal	75
4.2	Force production of WT and <i>dysf</i> -null lumbrical muscles	76
4.3	Normalized fluorescence intensities of FM1-43 during progression of lengthening contraction protocol	77
4.4	Intercontraction $[Ca^{2+}]_i$ during progression of lengthening contraction protocol	78

Abstract

Muscles exposed to unaccustomed exercise or injurious contractile activities are likely to sustain mechanical damage to muscle fibers, a characteristic of contraction-induced injuries. The susceptibility of muscles to contraction-induced injury increases with age, disuse or disease. Although lesions in the sarcolemma have been implicated in the injury process, the conditions that lead to the formation of such lesions, as well as the extent to which these lesions affect muscle function remain inadequately understood. To study membrane-based events reliably, we developed a micro-sized whole muscle model that was robust, but more importantly, compatible with the contemporary techniques used to study cellular function. In characterizing this muscle model *in vitro*, we report a level of stability and flexibility that had not been observed in previous whole muscle preparations. Utilizing this muscle model, we demonstrated that sarcolemmal lesions and overactive mechanosensitive ion channels accounted for the majority of the functional deficit observed in the diseased muscles of *mdx* mice, the murine model of Duchenne Muscular Dystrophy. These results provide a basis for the development of therapeutic strategies directed at stabilizing the membrane of dystrophic skeletal muscle. When wild-type muscles were subjected to an injurious protocol of lengthening contractions, the mechanical stress associated with lengthening contractions, while severe enough to cause

a 30% force deficit, was found to be insufficient to elicit membrane lesions in a whole skeletal muscle. This finding diminished the role of mechanical stress as the direct cause of sarcolemmal injury and implies that contraction-induced lesions observed in wild-type muscle are likely to result from the contributions of other factors, such as reactive oxygen species and proteolytic enzyme activity.

Chapter 1

Introduction

Overview

The human body contains approximately 630 skeletal muscles, accounting for ~40% of its mass (17). Skeletal muscles are capable of generating a wide diversity of forces and power that provide an extraordinary range of movements. The musculature in the lower limbs propel a sprinter to the finish line at a remarkable velocity, whereas the muscles in the palm of the hand enable a pianist to play the most delicate of concertos. For these reasons, a variety of scholars throughout history have demonstrated a high level of interest in muscle structure and function. Indeed, the earliest recorded scientific study of muscle function was undertaken by Claudius Galen (129-201 A.D.) over two thousand years ago. A physician to the Roman gladiators, Galen performed numerous dissections and experiments on animals and was the first to report on the basic function of muscles, nerves and vasculature.

The current understanding of muscle function has increased immeasurably since Galen's rudimentary experiments two millennia ago. Modern textbooks describe in remarkable detail the molecular mechanisms, mechanics and energy requirements for muscle activity (33). Muscle research continues to expand, fueled by technological breakthroughs in computing, imaging, mathematical modeling and genetics. Investigators

now have the scientific expertise to measure forces of single myosin molecules (14), deliver gene therapies to dystrophic mice (18) and simulate the behavior of muscles entirely *in silico** (39). Each of these achievements highlights the diverse accomplishments made in the pursuit of new knowledge regarding skeletal muscle structure and function.

Research Motivation and Approach

Injury to skeletal muscle fibers occurs as a result of trauma, disease, extreme temperature or exposure to myotoxins (6). Despite the potential for these interventions to cause injury, muscles most commonly sustain injuries resulting from exercise or contractile activity (35). This type of injury, termed a “contraction-induced injury”, is characterized by mechanical damage to force-generating components within muscle fibers that result in muscle soreness and an impaired ability of the muscle to generate force (11). While considerable progress has been achieved in this area of muscle research, the causal mechanisms of contraction-induced injuries remain incompletely understood. Advancements in the understanding of contraction-induced injuries can potentially exert an immediate impact across a wide variety of health issues, including muscular dystrophy and age-related muscle weakness of the elderly (4; 31). Patients that suffer from muscular dystrophy, as well as individuals from the elderly population, exhibit a pronounced susceptibility to contraction-induced injury (12; 57) and are consequently obliged to lead sedentary lifestyles. In addition to diminishing the quality of

* An expression used to mean "performed on computer or via computer simulation."

life, muscle-associated health issues also exert a substantial financial burden, estimated at ~\$15 billion annually from age-related muscle weakness alone (25).

Due to its complexity, the study of contraction-induced injury may be approached from a variety of perspectives. The research presented in this dissertation has focused specifically on the role of the plasma membrane in contraction-induced injuries. A membrane-based approach offers two distinct advantages. Firstly, potential therapeutics developed to target the membrane can exert their effects external to the cell, without a need for entry into the cytosol. This is advantageous from a drug delivery standpoint, as membrane-targeting drugs can bypass the complicated packaging techniques required for cellular uptake (27). Secondly, the elucidation of membrane-based events in a contraction-induced injury enables the development of treatment strategies aimed at stabilizing the injury-prone membranes of dystrophic muscle (38; 43). To provide a background for the research presented in subsequent chapters, a review of select areas of muscle function and physiology will be presented in the remaining portion of this introductory chapter.

The structure and function of skeletal muscles

Skeletal muscles consist of numerous cylindrical-shaped cells, known as muscle fibers, arranged parallel to one another. Depending on the organism and specific muscle, the number of muscle fibers in a whole skeletal muscle range from several hundred to several million (13). Each muscle fiber is a fully autonomous cell that contains highly specialized structures for force production. The fundamental basis of force generation is

derived from the interaction between two major sets of contractile proteins, the actin and myosin filaments (23). Spatially, each myosin filament is interdigitated with a hexagonal lattice of actin filaments; the overlap of actin and myosin filaments gives muscle its characteristic striated appearance (Fig 1.1). Surrounding these filaments is the sarcoplasmic reticulum (SR), an extensive membranous network that stores, releases and sequesters Ca^{2+} (2). During periods of quiescence, the basal concentration of intracellular Ca^{2+} is insufficient to elicit any interaction between actin and myosin filaments. When an action potential arrives at the muscle fiber, ion channels on the SR release Ca^{2+} into the cytosol that cause the concentration of Ca^{2+} in the myoplasm to increase ~ 200 fold (19). The Ca^{2+} exposes myosin-specific binding sites on the actin filaments that allow the two filaments to bind strongly to one another and form multiple cross-bridges. The movement of cross-bridges and their subsequent dissociation constitute the basis of the force-generating mechanism known as the cross bridge cycle (16) (Fig 1.2). Depending on the magnitude of the external load and the forces developed by the muscle fibers, contracting muscle fibers may either shorten, remain isometric, or lengthen (11).

In addition to the contractile apparatus, each muscle fiber is surrounded by an extensive network of supportive proteins and collagenous connective tissue (55) collectively known as the extracellular matrix (ECM). The ECM has three levels of organization; an endomysium that surrounds individual muscle fibers, a perimysium that encloses bundles of muscle fibers, and the epimysium that encompasses the entire muscle (49). The ECM transmits the forces generated by muscle fibers to the tendon as well as to adjacent muscle fibers (28; 46). Accordingly, the ECM can be regarded as a functional

link between muscle fibers and the skeleton (28). Mutations to proteins of the ECM result in two specific forms of muscular dystrophy, Congenital and Bethlem (8; 26), that highlight the importance of the ECM to muscle function.

The sarcolemma: the plasma membrane of muscle fibers

Fundamentally, cellular membranes serve as barriers to isolate cytosolic contents from the extracellular space. Through a finely-tuned system of channels, pumps and receptors, plasma membranes continuously regulate the concentration of ions in the cytosol to maintain an environment conducive for cellular processes (53; 56). In this regard, the sarcolemma behaves in a similar manner to that of the membranes of other eukaryotic cells. Indeed, several regulatory ion channels in the sarcolemma have homologous counterparts in the membranes of other cell types (42; 61). The mechanical properties of the sarcolemma are also similar to the membranes of other cell types and even artificial lipid bilayers (9; 10; 40). The functional resilience of the sarcolemma to mechanical stress is largely attributable to specialized protein complexes that are embedded periodically along the membrane of muscle fibers (3). These protein complexes, otherwise known as dystrophin-associated glycoprotein complexes (DGC), serve as membrane-bound connectors that link the contractile apparatus to ECM (3). These linkages impart mechanical stability to the sarcolemma by protecting it from the shear stresses developed in muscle fibers during contractile activity (22).

Characterization of a contraction-induced injury

Following unaccustomed physical activity, individuals commonly experience a delayed-onset of muscle soreness (DOMS), a phenomenon first recognized over a century ago (20). DOMS is indicative of a contraction-induced injury, with muscle soreness often accompanied by swelling (21) and efflux of intracellular enzymes from muscle fibers (50). Compared with shortening or isometric contractions, lengthening contractions are the only type of contractions that reproducibly causes injury in muscles (30; 36). The force deficit immediately after a severe, exhaustive protocol of lengthening contractions is attributable to both fatigue and injury, with the recovery from fatigue complete by ~3 hours (11). Depending on the severity of the contraction protocol, complete recovery from a contraction-induced injury may require durations from several weeks to 30 days (47). The overall progression of a contraction-induced injury is characterized by two distinct phases: an initial phase of injury ~0-12 hours after the protocol and a more severe secondary injury ~2-3 days later (11).

In the initial phase of a contraction-induced injury, the observed force deficit is largely attributable to mechanical damage to the force generating structures of muscle fibers (5; 15; 30). Electron micrographs of injured muscle fibers indicate a variety of severe ultrastructural abnormalities that include disrupted striation patterns and a displacement of actin and myosin filaments (5; 15; 30). In addition to ultrastructural damage, other factors also contribute to the initial force deficit, including disruption of the excitation-coupling system (54; 59) and activation of proteolytic factors (1).

In contrast to the initial injury, the force deficit in the secondary phase of contraction-induced injury is a result of oxidative stress (29; 62). Muscles exhibit overt morphological changes during the secondary phase of contraction-induced injury and portions of fibers at various stages of degeneration can be observed with conventional light microscopy (62). In severely damaged muscle fibers, a sealing-off process occurs around the site of injury that isolates the damaged region from the intact portions of the muscle fiber (36; 48). This sealing-off process ensures that only sufficiently damaged regions of the injured muscle fiber undergo repair. The sealed-off region gradually becomes contiguous with the extracellular space and attracts inflammatory cells that breakdown and remove cellular debris (36). Reactive oxygen species released by these inflammatory cells cause additional damage to uninjured muscle (45), accounting for the increase in force deficit during the secondary phase of contraction-induced injury (36; 62).

The role of calcium in muscle damage

Calcium plays a dual role in muscle function, serving as a signaling molecule as well as a regulator of muscle contraction and relaxation (2). To effectively regulate cytosolic $[Ca^{2+}]$, muscle fibers contain a complex system of channels, pumps and buffering proteins, each dedicated to mobilize, transport or sequester Ca^{2+} (2). A loss of Ca^{2+} homeostasis typically results in an accumulation of cytosolic Ca^{2+} that damages the muscle fiber via Ca^{2+} -activated free radical and enzymatic processes (17). These

destructive processes target the cytoskeleton and sarcolemma, and if left unchecked, could ultimately result in the necrosis of the entire muscle fiber (17; 52).

A loss in Ca^{2+} homeostasis can be triggered by a variety of interventions including hypoxia (34), osmotic stress (24) and prolonged contractile activity (32). The increase in resting cytosolic Ca^{2+} observed after prolonged contractile activity is partially attributable to Ca^{2+} influx through ion channels on the sarcolemma (42; 51). In addition to the ion channel pathway, Ca^{2+} may also enter through contraction-induced lesions in the sarcolemma (37; 41; 44). Presently, the mechanisms responsible for these contraction-induced lesions are still unclear, although mechanical stress has been proposed to play an important role (37; 41; 58). These lesions are likely to be significant contributors to the contraction-induced elevation of cytosolic Ca^{2+} , given the ~18,000 fold difference in Ca^{2+} concentration that exists across the membrane of quiescent muscle fibers (60).

Aims

The overall aim of this dissertation was to determine, in whole skeletal muscles, the contribution of discrete membrane lesions to contraction-induced injury, and in addition, examine the conditions that promote the formation of these lesions. All experiments were performed on a micro-sized whole muscle preparation that utilizes the lumbrical (LMB) muscle from the forepaw of a mouse. This miniature muscle model was largely based on the hindpaw LMB preparation developed previously by Claffin and Brooks (7).

To address the aims of the dissertation, three studies were performed and the results presented in chapters 2, 3 and 4, respectively. The goal of the first study was to characterize the LMB muscle from the forepaw and assess its potential as a model to study contractile activity. The second study utilized a membrane-patching polymer to determine the contribution of sarcolemmal lesions to the contraction-induced force deficits of dystrophic muscle. Results from this work motivated the development of the final study that sought to determine the extent to which contraction-induced lesions occurred in wild-type muscle.

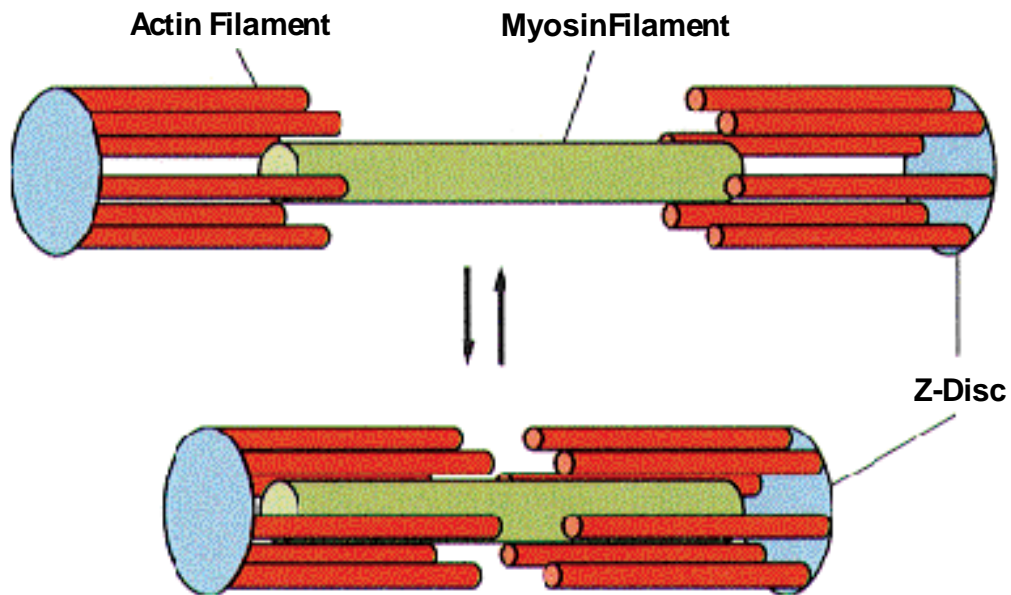


Figure 1.1. Spatial orientation of actin and myosin filaments. *Top:* Each myosin filament is interdigitated with a two hexagonal arrays of actin filaments. One end of each actin filament is attached directly to the Z-disc, a network of interconnecting proteins. Myosin filaments are attached to the Z-disc at both ends via a set of elastic proteins (not shown). *Bottom:* The movement of actin filaments towards the center of the myosin protein results in the contraction of muscle.

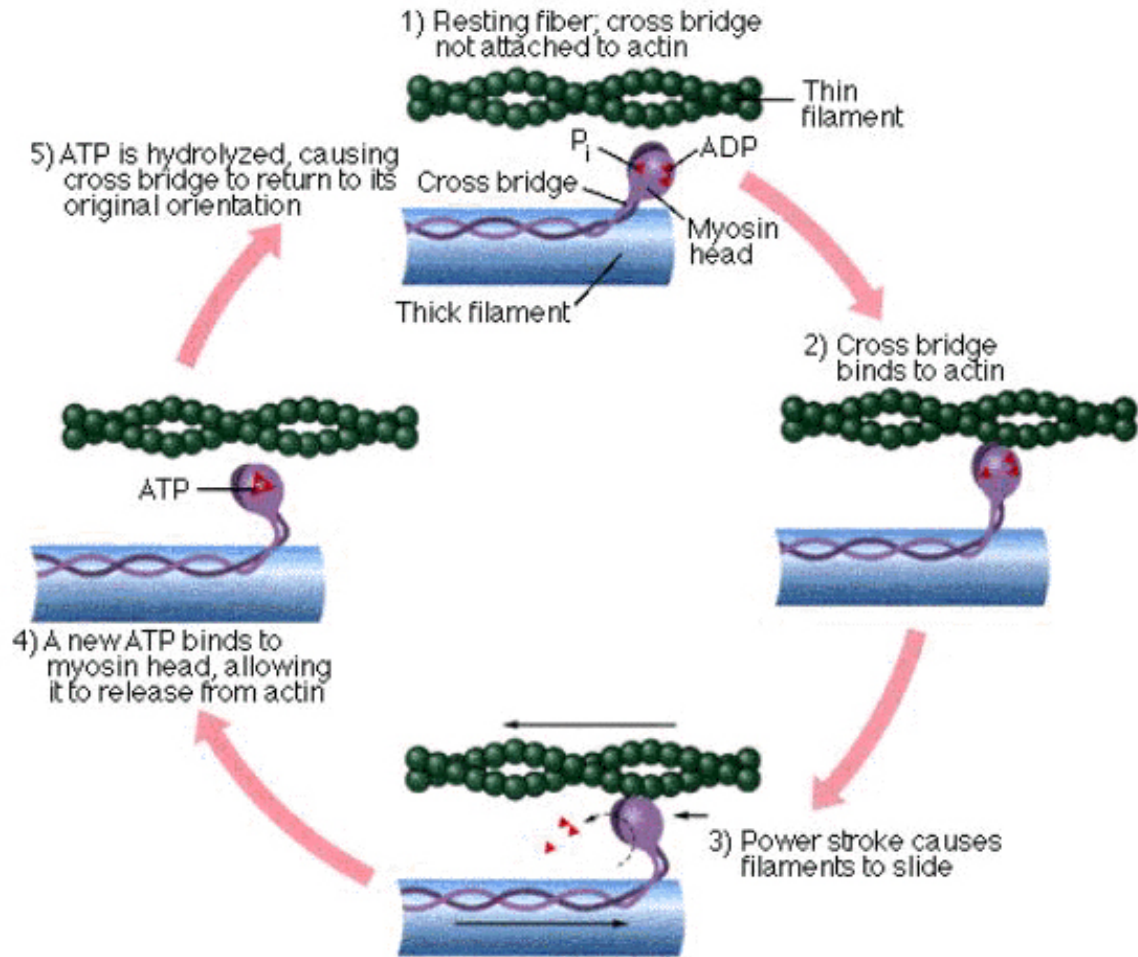


Figure 1.2. The cross bridge cycle. The cycle is initiated when the myosin head attaches to the actin filament (1→2). In the next phase, the myosin head pulls the actin filament, releasing ADP and inorganic phosphate in the process (2→3). The dissociation of the myosin head from the actin filament is induced by binding an ATP molecule (4). The ATP is then hydrolyzed and the cross bridge returns to its original conformation (5).

References

1. **Belcastro AN.** Skeletal muscle calcium-activated neutral protease (calpain) with exercise. *J Appl Physiol* 74: 1381-1386, 1993.
2. **Berchtold MW, Brinkmeier H and Muntener M.** Calcium ion in skeletal muscle: its crucial role for muscle function, plasticity, and disease. *Physiol Rev* 80: 1215-1265, 2000.
3. **Bloch RJ, Capetanaki Y, O'Neill A, Reed P, Williams MW, Resneck WG, Porter NC and Ursitti JA.** Costameres: repeating structures at the sarcolemma of skeletal muscle. *Clin Orthop Relat Res* S203-S210, 2002.
4. **Brooks SV and Faulkner JA.** Skeletal muscle weakness in old age: underlying mechanisms. *Med Sci Sports Exerc* 26: 432-439, 1994.
5. **Brooks SV, Zerba E and Faulkner JA.** Injury to muscle fibres after single stretches of passive and maximally stimulated muscles in mice. *J Physiol* 488 (Pt 2): 459-469, 1995.
6. **Carlson BM and Faulkner JA.** The regeneration of skeletal muscle fibers following injury: a review. *Med Sci Sports Exerc* 15: 187-198, 1983.

7. **Claffin DR and Brooks SV.** Direct observation of failing fibers in muscles of dystrophic mice provides mechanistic insight into muscular dystrophy. *Am J Physiol Cell Physiol* 294: C651-C658, 2008.
8. **Cohn RD, Herrmann R, Sorokin L, Wewer UM and Voit T.** Laminin alpha2 chain-deficient congenital muscular dystrophy: variable epitope expression in severe and mild cases. *Neurology* 51: 94-100, 1998.
9. **Evans E, Heinrich V, Ludwig F and Rawicz W.** Dynamic tension spectroscopy and strength of biomembranes. *Biophys J* 85: 2342-2350, 2003.
10. **Evans EA, Waugh R and Melnik L.** Elastic area compressibility modulus of red cell membrane. *Biophys J* 16: 585-595, 1976.
11. **Faulkner JA, Brooks SV and Opitck JA.** Injury to skeletal muscle fibers during contractions: conditions of occurrence and prevention. *Phys Ther* 73: 911-921, 1993.
12. **Faulkner JA, Brooks SV and Zerba E.** Skeletal muscle weakness and fatigue in old age: underlying mechanisms. *Annu Rev Gerontol Geriatr* 10: 147-166, 1990.
13. **Feinstein B, Lindegard B, Nyman E and Wohlfart G.** Morphologic studies of motor units in normal human muscles. *Acta Anat (Basel)* 23: 127-142, 1955.

14. **Finer JT, Simmons RM and Spudich JA.** Single myosin molecule mechanics: piconewton forces and nanometre steps. *Nature* 368: 113-119, 1994.
15. **Friden J, Sjostrom M and Ekblom B.** Myofibrillar damage following intense eccentric exercise in man. *Int J Sports Med* 4: 170-176, 1983.
16. **Geeves MA, Fedorov R and Manstein DJ.** Molecular mechanism of actomyosin-based motility. *Cell Mol Life Sci* 62: 1462-1477, 2005.
17. **Gissel H.** The role of Ca²⁺ in muscle cell damage. *Ann N Y Acad Sci* 1066: 166-180, 2005.
18. **Gregorevic P, Allen JM, Minami E, Blankinship MJ, Haraguchi M, Meuse L, Finn E, Adams ME, Froehner SC, Murry CE and Chamberlain JS.** rAAV6-microdystrophin preserves muscle function and extends lifespan in severely dystrophic mice. *Nat Med* 12: 787-789, 2006.
19. **Hollingworth S, Zhao M and Baylor SM.** The amplitude and time course of the myoplasmic free [Ca²⁺] transient in fast-twitch fibers of mouse muscle. *J Gen Physiol* 108: 455-469, 1996.
20. **Hough T.** Ergographic studies in muscular soreness. *Am J Physiol* 76-92, 2008.

21. **Howell JN, Chleboun G and Conatser R.** Muscle stiffness, strength loss, swelling and soreness following exercise-induced injury in humans. *J Physiol* 464: 183-196, 1993.
22. **Hutter OF.** The membrane hypothesis of Duchenne muscular dystrophy: quest for functional evidence. *J Inherit Metab Dis* 15: 565-577, 1992.
23. **Huxley AF.** Muscle structure and theories of contraction. *Prog Biophys Biophys Chem* 7: 255-318, 1957.
24. **Imbert N, Vandebrouck C, Constantin B, Duport G, Guillou C, Cognard C and Raymond G.** Hypoosmotic shocks induce elevation of resting calcium level in Duchenne muscular dystrophy myotubes contracting in vitro. *Neuromuscul Disord* 6: 351-360, 1996.
25. **Janssen I, Shepard DS, Katzmarzyk PT and Roubenoff R.** The healthcare costs of sarcopenia in the United States. *J Am Geriatr Soc* 52: 80-85, 2004.
26. **Jobsis GJ, Keizers H, Vreijling JP, de VM, Speer MC, Wolterman RA, Baas F and Bolhuis PA.** Type VI collagen mutations in Bethlem myopathy, an autosomal dominant myopathy with contractures. *Nat Genet* 14: 113-115, 1996.

27. **Juliano R.** Challenges to macromolecular drug delivery. *Biochem Soc Trans* 35: 41-43, 2007.
28. **Kjaer M.** Role of extracellular matrix in adaptation of tendon and skeletal muscle to mechanical loading. *Physiol Rev* 84: 649-698, 2004.
29. **Lapointe BM, Frenette J and Cote CH.** Lengthening contraction-induced inflammation is linked to secondary damage but devoid of neutrophil invasion. *J Appl Physiol* 92: 1995-2004, 2002.
30. **Lieber RL, Woodburn TM and Friden J.** Muscle damage induced by eccentric contractions of 25% strain. *J Appl Physiol* 70: 2498-2507, 1991.
31. **Lynch GS.** Role of contraction-induced injury in the mechanisms of muscle damage in muscular dystrophy. *Clin Exp Pharmacol Physiol* 31: 557-561, 2004.
32. **Lynch GS, Fary CJ and Williams DA.** Quantitative measurement of resting skeletal muscle $[Ca^{2+}]_i$ following acute and long-term downhill running exercise in mice. *Cell Calcium* 22: 373-383, 1997.
33. **MacIntosh B.R, Gardiner P. and McComas A.J.** *Skeletal Muscle: Form and Function.* Human Kinetics Publishers, 2005.

34. **McCall KE and Duncan CJ.** Independent pathways causing cellular damage in mouse soleus muscle under hypoxia. *Comp Biochem Physiol A* 94: 799-804, 1989.
35. **McCully KK.** Exercise-induced injury to skeletal muscle. *Fed Proc* 45: 2933-2936, 1986.
36. **McCully KK and Faulkner JA.** Injury to skeletal muscle fibers of mice following lengthening contractions. *J Appl Physiol* 59: 119-126, 1985.
37. **McNeil PL and Khakee R.** Disruptions of muscle fiber plasma membranes. Role in exercise-induced damage. *Am J Pathol* 140: 1097-1109, 1992.
38. **Menke A and Jockusch H.** Decreased osmotic stability of dystrophin-less muscle cells from the mdx mouse. *Nature* 349: 69-71, 1991.
39. **Nagano A, Komura T and Fukashiro S.** Optimal coordination of maximal-effort horizontal and vertical jump motions--a computer simulation study. *Biomed Eng Online* 6: 20, 2007.
40. **Nichol JA and Hutter OF.** Tensile strength and dilatational elasticity of giant sarcolemmal vesicles shed from rabbit muscle. *J Physiol* 493 (Pt 1): 187-198, 1996.

41. **Noakes TD.** Effect of exercise on serum enzyme activities in humans. *Sports Med* 4: 245-267, 1987.
42. **Parekh AB and Putney JW, Jr.** Store-operated calcium channels. *Physiol Rev* 85: 757-810, 2005.
43. **Pasternak C, Wong S and Elson EL.** Mechanical function of dystrophin in muscle cells. *J Cell Biol* 128: 355-361, 1995.
44. **Petrof BJ, Shrager JB, Stedman HH, Kelly AM and Sweeney HL.** Dystrophin protects the sarcolemma from stresses developed during muscle contraction. *Proc Natl Acad Sci U S A* 90: 3710-3714, 1993.
45. **Pizza FX, Peterson JM, Baas JH and Koh TJ.** Neutrophils contribute to muscle injury and impair its resolution after lengthening contractions in mice. *J Physiol* 562: 899-913, 2005.
46. **Purslow PP and Trotter JA.** The morphology and mechanical properties of endomysium in series-fibred muscles: variations with muscle length. *J Muscle Res Cell Motil* 15: 299-308, 1994.

47. **Rader EP and Faulkner JA.** Recovery from contraction-induced injury is impaired in weight-bearing muscles of old male mice. *J Appl Physiol* 100: 656-661, 2006.
48. **Rader EP, Song W, Van RH, Richardson A and Faulkner JA.** Raising the antioxidant levels within mouse muscle fibres does not affect contraction-induced injury. *Exp Physiol* 91: 781-789, 2006.
49. **Sane SF.** The extracellular matrix. In: *Myology*, edited by Andrew GE and Franzini-Armstrong C. New York: McGraw-Hill, Medical Publication Division, 1994, p. 242-260.
50. **Schwane JA, Johnson SR, Vandenakker CB and Armstrong RB.** Delayed-onset muscular soreness and plasma CPK and LDH activities after downhill running. *Med Sci Sports Exerc* 15: 51-56, 1983.
51. **Sonobe T, Inagaki T, Poole DC and Kano Y.** Intracellular calcium accumulation following eccentric contractions in rat skeletal muscle in vivo: role of stretch-activated channels. *Am J Physiol Regul Integr Comp Physiol* 294: R1329-R1337, 2008.
52. **Street SF and Ramsey RW.** Sarcolemma: transmitter of active tension in frog skeletal muscle. *Science* 149: 1379-1380, 1965.

53. **Strehler EE, Filoteo AG, Penniston JT and Caride AJ.** Plasma-membrane Ca(2+) pumps: structural diversity as the basis for functional versatility. *Biochem Soc Trans* 35: 919-922, 2007.
54. **Takekura H, Fujinami N, Nishizawa T, Ogasawara H and Kasuga N.** Eccentric exercise-induced morphological changes in the membrane systems involved in excitation-contraction coupling in rat skeletal muscle. *J Physiol* 533: 571-583, 2001.
55. **Trotter JA and Purslow PP.** Functional morphology of the endomysium in series fibered muscles. *J Morphol* 212: 109-122, 1992.
56. **Vigh L, Nakamoto H, Landry J, Gomez-Munoz A, Harwood JL and Horvath I.** Membrane regulation of the stress response from prokaryotic models to mammalian cells. *Ann N Y Acad Sci* 1113: 40-51, 2007.
57. **Wagner KR, Lechtzin N and Judge DP.** Current treatment of adult Duchenne muscular dystrophy. *Biochim Biophys Acta* 1772: 229-237, 2007.
58. **Warren GL, Hayes DA, Lowe DA and Armstrong RB.** Mechanical factors in the initiation of eccentric contraction-induced injury in rat soleus muscle. *J Physiol* 464: 457-475, 1993.

59. **Warren GL, Lowe DA, Hayes DA, Karwoski CJ, Prior BM and Armstrong RB.** Excitation failure in eccentric contraction-induced injury of mouse soleus muscle. *J Physiol* 468: 487-499, 1993.

60. **Williams DA, Head SI, Bakker AJ and Stephenson DG.** Resting calcium concentrations in isolated skeletal muscle fibres of dystrophic mice. *J Physiol* 428: 243-256, 1990.

61. **Yang XC and Sachs F.** Block of stretch-activated ion channels in *Xenopus* oocytes by gadolinium and calcium ions. *Science* 243: 1068-1071, 1989.

62. **Zerba E, Komorowski TE and Faulkner JA.** Free radical injury to skeletal muscles of young, adult, and old mice. *Am J Physiol* 258: C429-C435, 1990.

Chapter 2

The benefits of a miniature whole muscle model for studies of prolonged, repetitive contractile activity *in vitro*

Abstract

Whole muscle preparations offer uncomplicated and reliable models for the study of muscle function *in vitro*. Despite their utility, whole muscle models such as the soleus or EDL muscle frequently remain too large for the application of contemporary imaging techniques. In addition, these muscles require long and often uncertain incubation periods for the equilibration of externally-applied macromolecular compounds. In the present study, we describe the development of an extremely small whole muscle preparation that overcomes the traditional limitations associated with whole muscle models. This miniature muscle preparation utilizes the lumbrical muscle (LMB) from the forepaw of the mouse that has a cross sectional area $\sim 1/25^{\text{th}}$ that of an EDL muscle. When subjected to a protocol of 900 isometric contractions, the LMB muscles maintained force production throughout a 30 min test period and showed no signs of fatigue, or deterioration. In contrast, when LMB muscles were subjected to 900 lengthening contractions, a 20% post-protocol force deficit occurred with overt damage to individual muscle fibers. The injury was easily visualized with Evans Blue Dye, while the muscle remained *in vitro*. In addition to force deficit measurements, quantification of muscle

damage was achieved through fluorescence measurements of FM1-43. Overall, the LMB muscles proved to be: (i) compatible with fluorescence techniques, (ii) sufficiently small to enhance the diffusion of macromolecules and (iii) stable even under severe metabolic demands. These features qualify the LMB muscle as a flexible and robust model for the study of prolonged contractile activity *in vitro*.

Introduction

The consistency, flexibility and overall control that the investigator has over *in vitro* muscle preparations has resulted in such muscle models becoming commonplace in many laboratories. *In vitro* models of mature skeletal muscles generally utilize either single muscle fibers (10; 15), or whole muscles (2), with each model possessing a distinct set of strengths and weaknesses. Compared with single muscle fibers, whole muscle models are easier to prepare in terms of the sophistication of the dissection required and offer a more accurate representation of physiological responses of muscles functioning *in vivo*. Despite these advantages, most whole muscle models are bulky and consequently require long and often uncertain incubation periods with dyes (7; 23), or macromolecular compounds. In addition, the large sizes of whole muscle models exclude the practical use of live cell fluorescence microscopy, a technique that is now utilized routinely in many areas of biological research (12; 17). The incompatibility of large whole muscles with such fluorescence techniques imposes a significant restriction on the utility of whole muscle models.

Recognizing the potential research impact that could be achieved from the miniaturization of whole muscle models, we developed a micro-sized whole muscle preparation that utilizes the lumbrical (LMB) muscle located in the fore-paw of a mouse. LMB muscles possess a cross-sectional area $\sim 1/25^{\text{th}}$ that of the extensor digitorum longus (EDL) muscle (4) and, by virtue of their small size, is able to retain much of the diffusion visualization benefits associated with single muscle fiber preparations. We have demonstrated previously the compatibility of LMB muscles with fluorescence techniques (5), as well as their effectiveness in incorporating macromolecular compounds (19). The purpose of the present study was to characterize the LMB muscle preparation based on an assessment of its potential as a model for the study of prolonged contractile activity *in vitro*. LMB muscles were divided into two groups and subjected to a protocol of either 900 isometric or 900 lengthening contractions over a 30 min test period. Injury to LMB muscles was assessed by force measurements, as well as visualization with Evans Blue Dye and fluorescent indicator FM1-43, a lipophilic, membrane-impermeable dye that fluoresces when partitioned into membranes (6).

Methods

Specific-pathogen-free male C57BL/6 mice 7-15 months of age were obtained from the Jackson Laboratory (Bar Harbor, ME). Mice were housed in a specific-pathogen-free barrier facility at the University of Michigan. All experimental procedures were approved by the University of Michigan Committee on the Use and Care of Animals and in accordance with the *Guide for the Care and Use of Laboratory Animals* [DHHS

Publication No. 85-23 (NIH), Revised 1985, Office of Science and Health Reports, Bethesda, MD 20892].

Operative procedure

Mice were anesthetized with an intraperitoneal injection of Avertin (tribromoethanol 400mg/kg). Supplemental doses of Avertin were administered as required to keep the mouse unresponsive to tactile stimuli. The front paws were severed from the mice and the lumbrical (LMB) muscles dissected free from the third digit. The mice were subsequently euthanized by an overdose of Avertin followed by a thoracotomy. Dissections were performed in a chilled bathing solution (approx. 8°C), with a composition in mM of: 137 NaCl, 11.9 NaHCO₃, 5.0 KCl, 1.8 CaCl₂, 0.5 MgCl₂, 0.4 NaH₂PO₄. The isolated LMB muscle was mounted horizontally in a custom-fabricated chamber with the distal tendon attached to a force transducer (Aurora Scientific, Inc., modified Model 400A) and the proximal tendon to a servomotor (Aurora Scientific, Inc., Model 318B). The ties were composed of 10-0 monofilament nylon suture. Bath temperature was maintained at 25°C and the chamber was perfused continuously with Tyrode solution, with a composition in mM of: 121 NaCl, 24 NaHCO₃, 5.0 KCl, 1.8 CaCl₂, 0.5 MgCl₂, 0.4 NaH₂PO₄. A pH of 7.3 was maintained by bubbling with a gas mixture of 95% O₂ and 5% CO₂.

Contractility measurements and contraction protocol

Muscles were stimulated electrically by current passed between two platinum plate electrodes. The constant-current stimulation pulses were 0.5 ms in duration and their magnitude was adjusted to elicit a maximum twitch response. Optimum length (L_o) of each muscle was determined by adjusting muscle length until maximum twitch force was attained. LMB muscles were sufficiently small that individual fibres could be discerned, allowing the length of muscle fibres (L_f) to be determined visually when the muscle was at L_o . To achieve a maximum isometric tetanic contraction, the muscle was stimulated with supramaximal intensity and frequency using pulses of alternating polarity. The specific force of each LMB muscle was calculated by dividing the maximum isometric force by an average cross-sectional area of 0.049 m^2 , a value obtained from the estimation of the diameter of four LMB muscles (with the assumption of a circular cross-section).

To simulate prolonged contractile activity *in vitro*, LMB muscles were divided into two groups and subjected to either 900 isometric (IC, n=4), or 900 lengthening (LC, n=8) contractions. Each contraction was 100 ms in duration and spaced at 2 s intervals, resulting in 30 min of continuous contractile activity. For the lengthening contractions, a stretch of 5% L_f was applied 40 ms after the start of stimulation and the muscle was subsequently returned to L_o at $1.25 L_f/s$.

Measurements of fluorescence from FM1-43

Muscles were exposed to FM1-43 (2.5 μ M in Tyrodes solution) after cessation of the contraction protocol. Fluorescence intensity measurements were collected from an area 1.1 mm by 0.23 mm along the length of the muscle and sampled periodically until no further increase in fluorescence intensity was noted. This final measurement was assigned as the fluorescence value for the muscle. Fluorescence was elicited by epi-illumination from a 75 W xenon lamp and detected using a photometer system (Photon Technology International, model Deltascan 4000). Excitation wavelength was selected using a diffraction grating monochromator and was centered at 479 nm (bandwidth 2 nm). The emitted fluorescence passed through a longpass filter (520 nm) before reaching the photomultiplier tube for detection.

Statistics

Data are presented as a mean value \pm SEM. Statistical analyses were performed using analysis of variance (ANOVA) with the level of significance set *a priori* at $P < 0.05$. When significance was detected, the Holm-Sidak post hoc comparison was applied.

Results

Force Production

The absolute and specific forces measured before the contraction protocol began were not different for the IC and LC groups. Pooling of the data yielded an average absolute force value of 12.1 ± 0.8 mN and a specific force of 247 ± 16 kN/m² (n=12).

Throughout the contraction protocol, muscles in the IC group generated forces that were not different from the initial time point (Fig 2.1B). In contrast, muscles in the LC group exhibited a rapid decline in force production and yielded a force deficit of ~50% immediately after the 900 LC protocol (Fig 2.1B). This force deficit was reduced to ~20% after a recovery period of 5 min and an additional period of recovery yielded no further reduction (Fig 2.1B). The recovery in force observed in the LC group is unlikely due to fatigue, as muscles in the IC group shared an identical duty cycle and did not demonstrate fatigue. The partial recovery of the force deficit following a non-fatiguing lengthening contraction protocol has been reported previously (3), and is not well understood. We propose that this partial recovery results from the realignment of disrupted contractile proteins.

Physical appearance of LMB muscles following repetitive lengthening contractions

After the LC protocol, LMB muscles showed overt signs of injury in a subpopulation of muscle fibers (Fig 2.2). A ~3 min incubation with Evans Blue Dye allowed visualization of the injury, which appeared as regions of myoplasmic separation and hypercontracture (Fig 2.2). The basement membrane of these injured muscle fibers appeared to remain intact, despite the retraction of large segments within the fiber. Injured muscle fibers resembled the “retraction clots” observed in single muscle fibers that sustained puncture wounds to the sarcolemma (21; 22). When incubated with FM1-43, the dye showed strong localization to the hypercontracted regions of muscle fibers (Fig 2.2). Due to its lipophilic nature (6), FM1-43 was likely to have bound selectively to

the aggregated plasma membranes in these contracture clots. Comparisons between muscles from IC and LC groups revealed that muscles in the LC group produced a fluorescence signal that was ~50% more intense than that observed for the IC group (Fig 2.3).

Discussion

LMB muscles remain viable during prolonged contractile activity in vitro

The robustness of the LMB muscle was demonstrated by its ability to maintain force production throughout the 30 min protocol of 900 isometric contractions. We are not aware of any other *in vitro* muscle preparation that behaves in a comparable manner. Typical muscle models, such as the extensor digitorum longus (EDL) muscle, show signs of fatigue even under less demanding contraction protocols (18; 19). The enhanced stability of the LMB muscle preparation is likely to be attributed to its small size that facilitates the movement of metabolites to and from the core of the muscle. The stability of the LMB muscles provides a strong endorsement for the application of this model to study repetitive contractile activity, or other aspects of muscle function that require prolonged experimentation *in vitro* (11; 20).

Size-associated benefits of LMB muscles

LMB muscles were sufficiently small to allow individual muscle fibers to be discerned *in vitro*, which permitted the use of fluorescence techniques to study muscle function or, in the case of the present study, assess damage. Utilizing FM1-43, we

demonstrated that the damage associated with contraction-induced injuries may be quantified by a fluorescence-based assay that provides a useful supplement to force deficit measurements. Compared with the measurements of force deficits, fluorescence-based assays are likely to provide a more specific and sensitive indication of muscle damage. The compatibility of LMB muscles with live fluorescence microscopy raises an exciting prospect for the application of fluorescent probes to elucidate various aspects of muscle function.

The short diffusion distance associated with LMB muscles is also particularly advantageous in experiments that utilize bulky, macromolecular compounds. This is because the time required for external compounds to reach the core of the muscle varies inversely with the square of its radius (8). This benefit is exemplified by the rapid ~3 min equilibration period with Evans Blue Dye; an incubation period that is ~20 times shorter than the existing 45-60 min required for whole muscle models such as the EDL or soleus (7; 23).

Comparison with in vivo models of repetitive contractile activity

As a means to validate the LMB muscle model, we compared the extent of damage observed in LMB muscles with those induced by downhill running exercise, a method used frequently to administer repetitive lengthening contractions to skeletal muscles of rodents (1; 13; 14; 16). Histological examination of muscles injured by downhill running exercises reveal an extent of damage that is less severe compared with the present protocol of repetitive lengthening contractions administered *in vitro* (1; 13;

16). We attribute this disparity to the milder forms of contractile activity associated with voluntary downhill running protocols. Muscles are activated sub-maximally during voluntary exercise, with recruitment of only a small proportion of the total motor units present in the muscle (9). The conditions *in vitro* are more severe, as all muscle fibers are activated maximally during each contraction for the entire duration of the exercise period. These differences are likely to account for the increased instances of overt damage to muscle fibers observed in the present study.

Conclusion

While the scope of the present study has been limited to contraction-induced injury, we are confident that the utility of the LMB muscle preparation can be extended to study almost all aspects of muscle research. We have established this unique micro-sized muscle preparation to be: (i) compatible with fluorescence techniques (ii) sufficiently small to promote the diffusion of dyes and macromolecules (19), and (iii) stable even during rigorous contractile protocols.

Acknowledgments

The authors thank Dennis Claflin and Susan Brooks for helpful discussions on the manuscript. This work was supported by grants AG000114, AG013283 and AG015434 from the National Institute of Health.

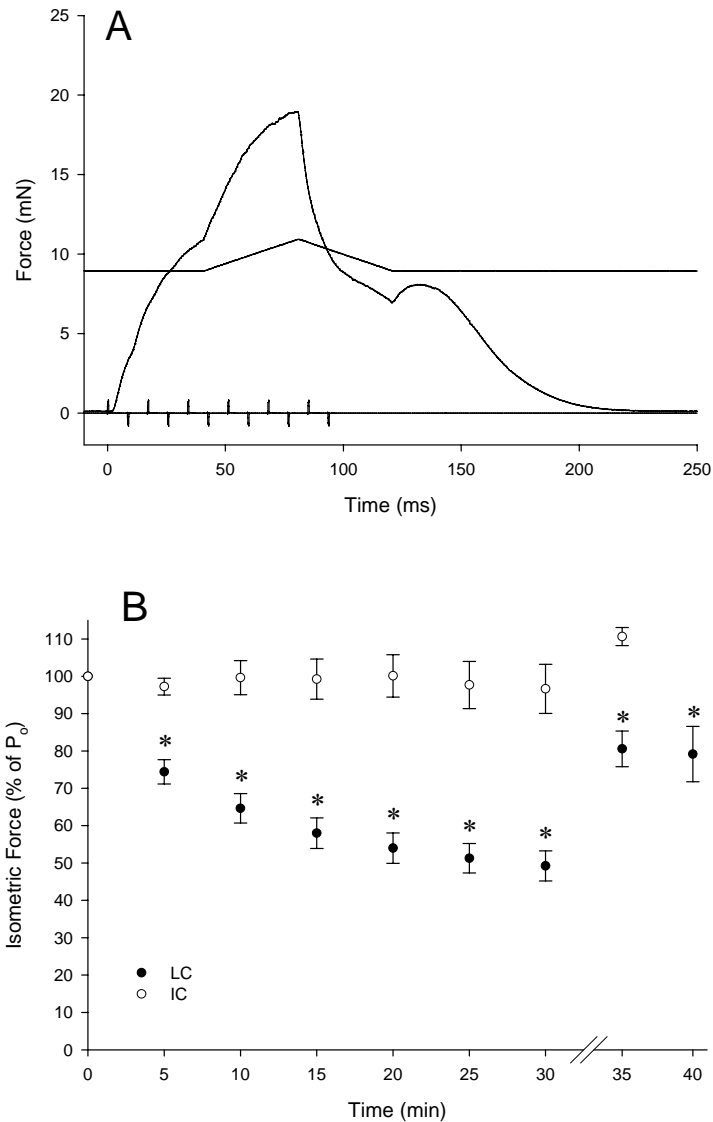


Fig 2.1 Force production of LMB muscles. *Top*: Example record of a typical force trace shown alongside stimulation and lengthening parameters. For clarity, only units of force is represented. *Bottom*: Force production during a 30 min protocol of 900 contractions. IC and LC denote isometric and lengthening contractions, respectively. Muscles in the IC group generated forces that were not different from the initial time point (Power > 0.8). Muscles in the LC group exhibited a force deficit of ~50% immediately after the lengthening contraction protocol that recovered to ~20% after a recovery period. Break along x-axis denotes the cessation of contractile activity. * indicates a difference when compared with the initial time point ($P < 0.05$).

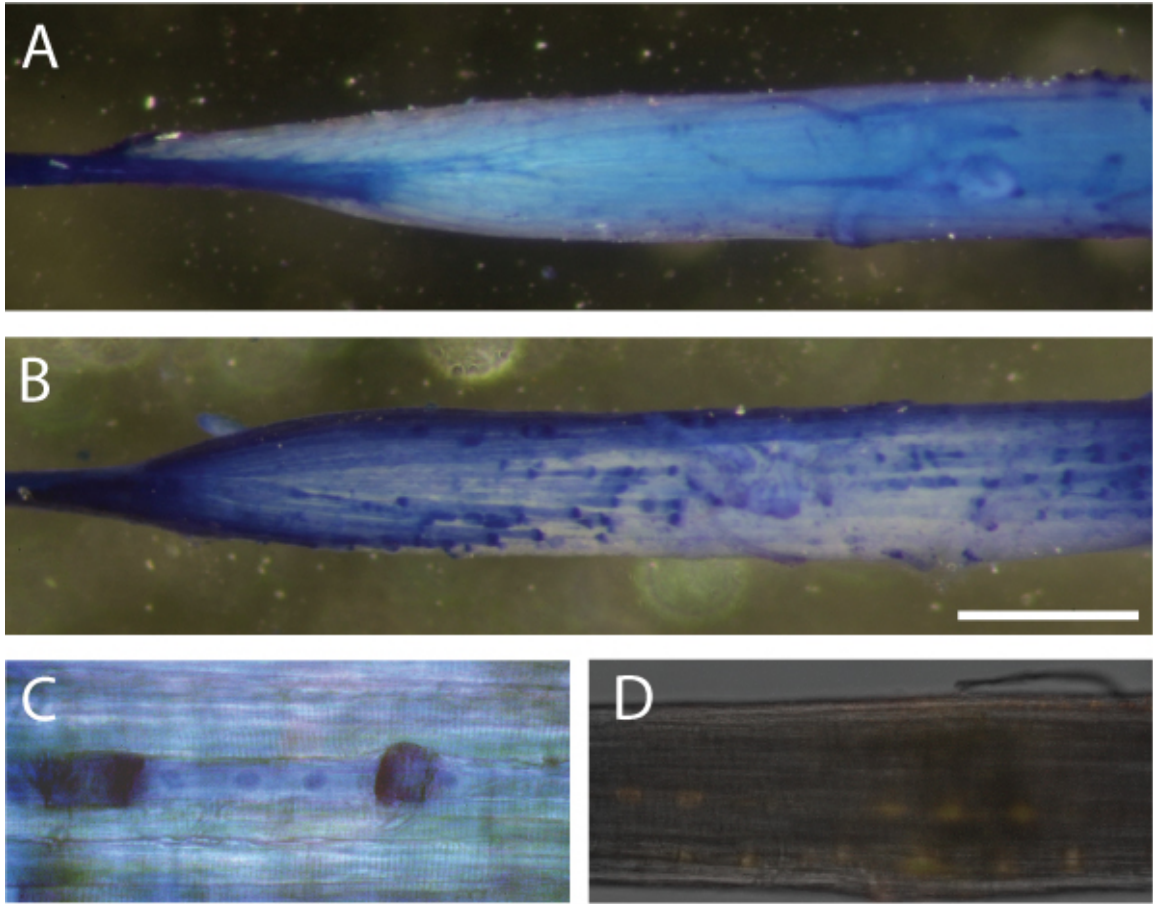


Fig 2.2. Visualization of injured muscle fibers with Evans Blue Dye ($4.6\mu\text{M}$, ~ 3 min incubation, panels A-C) and FM1-43 (panel D). Images were captured using a digital still camera and brightness/contrast modifications made using image editing software. (A) LMB muscle after a protocol of 900 isometric contractions. (B) LMB muscle after 900 lengthening contractions. Muscle exhibits overt injury to individual muscle fibers clearly visualized by Evans Blue Dye. Scale bar is $300\mu\text{m}$. (C) Close up of a damaged muscle fiber showing regions of myoplasmic separation. Note that the basement membrane still appears intact, and also the presence of striation patterns in adjacent, uninjured muscle fibers. (D) Brightfield image of LMB muscle after lengthening contractions superimposed with a fluorescent image of lipophilic dye FM1-43. Images reveal a localization of FM1-43 to hypercontracted muscle fibers.

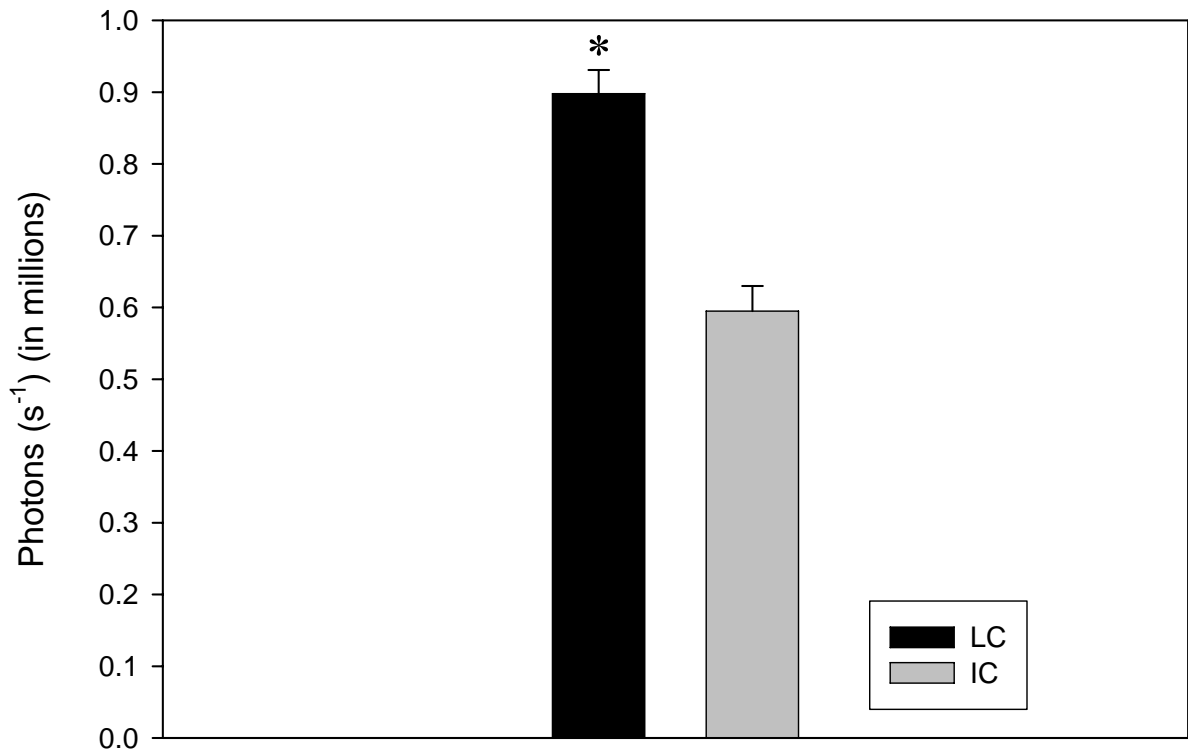


Fig 2.3. Measurements of FM1-43 intensity in muscles from IC and LC groups. LMB muscles were incubated with FM1-43 (2.5 μ M) after a protocol of either 900 isometric (IC) or lengthening contractions (LC). Fluorescence intensity measurements were collected from an area 1.1 mm by 0.23 mm along the length of the muscle. * indicates a difference when compared with the IC group ($P < 0.05$).

References

1. **Armstrong RB, Ogilvie RW and Schwane JA.** Eccentric exercise-induced injury to rat skeletal muscle. *J Appl Physiol* 54: 80-93, 1983.
2. **Brooks SV, Faulkner JA and McCubbrey DA.** Power outputs of slow and fast skeletal muscles of mice. *J Appl Physiol* 68: 1282-1285, 1990.
3. **Brooks SV, Zerba E and Faulkner JA.** Injury to muscle fibres after single stretches of passive and maximally stimulated muscles in mice. *J Physiol* 488 (Pt 2): 459-469, 1995.
4. **Burkholder TJ, Fingado B, Baron S and Lieber RL.** Relationship between muscle fiber types and sizes and muscle architectural properties in the mouse hindlimb. *J Morphol* 221: 177-190, 1994.
5. **Clafin DR and Brooks SV.** Direct observation of failing fibers in muscles of dystrophic mice provides mechanistic insight into muscular dystrophy. *Am J Physiol Cell Physiol* 294: C651-C658, 2008.
6. **Cochilla AJ, Angleson JK and Betz WJ.** Monitoring secretory membrane with FM1-43 fluorescence. *Annu Rev Neurosci* 22: 1-10, 1999.

7. **Consolino CM and Brooks SV.** Susceptibility to sarcomere injury induced by single stretches of maximally activated muscles of mdx mice. *J Appl Physiol* 96: 633-638, 2004.
8. **Hill AV.** Diffusion of Oxygen Through Tissues. In: *Trails and Trials in Physiology*, Baltimore, MD: Williams & Wilkins, 1965, p. 208-241.
9. **Hodson-Tole EF and Wakeling JM.** Motor unit recruitment patterns 1: responses to changes in locomotor velocity and incline. *J Exp Biol* 211: 1882-1892, 2008.
10. **Hollingworth S, Zhao M and Baylor SM.** The amplitude and time course of the myoplasmic free [Ca²⁺] transient in fast-twitch fibers of mouse muscle. *J Gen Physiol* 108: 455-469, 1996.
11. **Huang J, Hove-Madsen L and Tibbits GF.** SR Ca²⁺ refilling upon depletion and SR Ca²⁺ uptake rates during development in rabbit ventricular myocytes. *Am J Physiol Cell Physiol* 293: C1906-C1915, 2007.
12. **Jaiswal JK and Simon SM.** Imaging single events at the cell membrane. *Nat Chem Biol* 3: 92-98, 2007.
13. **Komulainen J, Kytola J and Vihko V.** Running-induced muscle injury and myocellular enzyme release in rats. *J Appl Physiol* 77: 2299-2304, 1994.

14. **Lynch GS, Fary CJ and Williams DA.** Quantitative measurement of resting skeletal muscle $[Ca^{2+}]_i$ following acute and long-term downhill running exercise in mice. *Cell Calcium* 22: 373-383, 1997.
15. **Lynch GS, Rafael JA, Chamberlain JS and Faulkner JA.** Contraction-induced injury to single permeabilized muscle fibers from mdx, transgenic mdx, and control mice. *Am J Physiol Cell Physiol* 279: C1290-C1294, 2000.
16. **McNeil PL and Khakee R.** Disruptions of muscle fiber plasma membranes. Role in exercise-induced damage. *Am J Pathol* 140: 1097-1109, 1992.
17. **Miyawaki A, Sawano A and Kogure T.** Lighting up cells: labelling proteins with fluorophores. *Nat Cell Biol Suppl*: S1-S7, 2003.
18. **Moens P, Baatsen PH and Marechal G.** Increased susceptibility of EDL muscles from mdx mice to damage induced by contractions with stretch. *J Muscle Res Cell Motil* 14: 446-451, 1993.
19. **Ng R, Metzger JM, Claflin DR and Faulkner JA.** Poloxamer 188 reduces the contraction-induced force decline in lumbrical muscles from *mdx* mice. *Am J Physiol Cell Physiol* 2008.

20. **Patel N, Huang C and Klip A.** Cellular location of insulin-triggered signals and implications for glucose uptake. *Pflugers Arch* 451: 499-510, 2006.
21. **Rapoport SI.** The anisotropic elastic properties of the sarcolemma of the frog semitendinosus muscle fiber. *Biophys J* 13: 14-36, 1973.
22. **Street SF and Ramsey RW.** Sarcolemma: transmitter of active tension in frog skeletal muscle. *Science* 149: 1379-1380, 1965.
23. **Whitehead NP, Streamer M, Lusambili LI, Sachs F and Allen DG.**
Streptomycin reduces stretch-induced membrane permeability in muscles from mdx mice. *Neuromuscul Disord* 16: 845-854, 2006.

Chapter 3

Poloxamer 188 reduces the contraction-induced force decline in lumbrical muscles from *mdx* mice

Abstract

Duchenne Muscular Dystrophy is a genetic disease caused by the lack of the protein dystrophin. Dystrophic muscles are highly susceptible to contraction-induced injury, and following contractile activity, have disrupted plasma membranes that allow leakage of calcium ions into muscle fibers. Because of the direct relationship between increased intracellular calcium concentration and muscle dysfunction, therapeutic outcomes may be achieved through the identification and restriction of calcium influx pathways. Our purpose was to determine the contribution of sarcolemmal lesions to the force deficits caused by contraction-induced injury in dystrophic skeletal muscles. Using isolated lumbrical muscles from dystrophic (*mdx*) mice, we demonstrate for the first time that P188, a membrane sealing poloxamer, is effective in reducing the force deficit in a whole *mdx* skeletal muscle. A reduction in force deficit was also observed in *mdx* muscles that were exposed to a calcium-free environment. These results, coupled with previous observations of calcium entry into *mdx* muscle fibers during a similar contraction protocol, support the interpretation that extracellular calcium enters through sarcolemmal lesions and contributes to the force deficit observed in *mdx* muscles. The

results provide a basis for potential therapeutic strategies directed at membrane stabilization of dystrophin-deficient skeletal muscle fibers.

Introduction

Duchenne Muscular Dystrophy (DMD) is an X-linked genetic disease caused by a mutation in the dystrophin gene. As a result, muscles from patients with DMD lack dystrophin, a 427 kDa protein located beneath the cytoplasmic surface of the plasma membrane, the sarcolemma, of muscle fibers (5). Dystrophin is required for the assembly of the dystrophin-associated glycoprotein complex that is embedded in the sarcolemma (26). The dystrophin-glycoprotein complex links the actin cytoskeleton to the basement membrane and is thought to provide mechanical stability to the sarcolemma (19; 28). Although the exact function of dystrophin is still unknown, the pathology demonstrated by skeletal muscles of young males that lack dystrophin is dramatic. Boys with DMD experience progressive muscle weakness beginning at about 2-5 years of age, are wheelchair bound by age 12, and die in their mid-twenties from respiratory or cardiac failure (17).

The *mdx* mouse, discovered in 1984 (9), does not express dystrophin and consequently provides an important animal model for studying the effects of dystrophin deficiency. Studies performed on muscles from the *mdx* mouse, hereafter termed *mdx* muscles, have documented impairments in structure and function, including a high susceptibility to contraction-induced injury (11; 15; 21). We have shown previously that force deficits produced by contraction-induced injury to *mdx* muscles are associated with

an influx of extracellular calcium into muscle fibers (11). Stretch-activated, store-operated and calcium leak channels have been implicated as entry sites responsible for the influx of extracellular calcium (6; 13; 35). However, these ion channels are unlikely to be entirely responsible for the calcium influx since bulky, membrane impermeable dyes and enzymes also traverse the sarcolemma of dystrophic muscles (1; 29; 30). These observations suggest the involvement of larger, nonspecific calcium entry pathways in the membrane, such as sarcolemmal lesions.

Poloxamer 188 (P188) is an 8.4 kDa amphiphilic polymer that localizes into lipid monolayers (33) and damaged portions of membranes (22). When applied to injured cells, P188 repairs disrupted membranes and enhances the recovery of skeletal muscle (20), fibroblasts (25), cardiac myocytes (34) and the spinal cord (7) from a variety of injury-inducing protocols. Our purpose was to determine, through the application of P188, the extent to which sarcolemmal lesions are responsible for the increased susceptibility of dystrophic skeletal muscles to contraction-induced injury. To minimize concerns regarding non-uniform intramuscular distribution of the applied compounds, we utilized the lumbrical (LMB) muscle, a very small whole muscle located in the forepaw of the mouse. LMB muscles were treated with P188 and then subjected to an isometric contraction protocol *in vitro* that produced a force deficit in untreated *mdx* muscles. We hypothesized that the force deficits would be highest in untreated dystrophic muscles, intermediate in dystrophic muscles treated with P188, and lowest in wild-type muscles

Methods

Specific-pathogen-free male *mdx* mice (C57BL/10ScSn-*mdx* stock #001801) 2-3 months of age and wild-type (WT) C57BL/10 mice 2-5 months of age were obtained from the Jackson Laboratory (Bar Harbor, ME). Mice were housed in a specific-pathogen-free barrier facility at the University of Michigan. All experimental procedures were approved by the University of Michigan Committee on the Use and Care of Animals and in accordance with the *Guide for the Care and Use of Laboratory Animals* [DHHS Publication No. 85-23 (NIH), Revised 1985, Office of Science and Health Reports, Bethesda, MD 20892].

LMB muscle as a model to study contraction-induced injury in vitro

The use of a small muscle such as the LMB minimizes the demands made on diffusion processes that may arise when using a larger whole muscle. The shorter diffusion paths of the small muscle facilitate the movement of metabolites to and from its core, maintaining its viability *in vitro*. Throughout the course of the experiments, LMB muscles of WT mice exhibited a sustained ability to maintain force, a positive indication of the overall stability of the muscle. The initial experimental design included a parallel set of experiments on the more commonly used extensor digitorum longus muscle (EDL). During these experiments, the EDL exhibited fatigue, with a ~10% loss in force after 10 isometric contractions followed by a full recovery of force after a rest period of 10 min (see Supplementary Materials). Since our goal was to investigate contraction-induced

injury in the absence of confounding factors such as loss of force due to fatigue, the experiments on the EDL muscles were discontinued.

The shorter diffusion distance associated with small muscles is also advantageous in drug-based experiments, particularly when macromolecules such as P188 are tested. This is because the time required for the concentration of a compound at the core of the muscle to reach 50% of its concentration in the bathing medium is proportional to the square of the radius of the muscle (16). For example, the LMB muscle with a typical radius of 150 μ m would require a diffusion time that is 16-fold less than the EDL muscle that has a typical radius of 600 μ m (10).

Intact single muscle fibers circumvent diffusion-based problems and have been used to study the effects of membrane-targeting compounds in *mdx* muscles (35). Despite advantages for drug distribution, the behavior of an isolated single muscle fiber without interactions with adjacent muscle fibers might not provide an accurate representation of the function of a whole muscle. A small whole muscle such as the LMB retains some of the diffusion benefits and visualization advantages normally accorded to single muscle fiber preparations, while maintaining a more accurate representation of *in vivo* whole muscle function.

Operative procedure

Mice were anesthetized with an intraperitoneal injection of Avertin (tribromoethanol 400mg/kg). Supplemental doses of Avertin were administered as required to keep the mouse unresponsive to tactile stimuli. The front paws were severed

from the mice and the LMB muscles dissected free from the third digit. The mice were subsequently euthanized by an overdose of Avertin followed by a thoracotomy. Dissections were performed in a chilled bathing solution (approx. 8°C), composition in mM: 137 NaCl, 11.9 NaHCO₃, 5.0 KCl, 1.8 CaCl₂, 0.5 MgCl₂, 0.4 NaH₂PO₄. Based on physical dimensions, LMB muscle mass was estimated to be approximately 0.2 mg. The isolated LMB muscle was mounted horizontally in a custom-fabricated chamber with the distal tendon attached to a force transducer (Aurora Scientific, Inc., modified Model 400A) and the proximal tendon to a servomotor (Aurora Scientific, Inc., Model 318B). The ties were composed of 10-0 monofilament nylon suture. Bath temperature was maintained at 25°C and the chamber was perfused continuously with Tyrode solution (composition in mM: 121 NaCl, 24 NaHCO₃, 5.0 KCl, 1.8 CaCl₂, 0.5 MgCl₂, 0.4 NaH₂PO₄). A pH of 7.3 was maintained by bubbling with a 95%/5% O₂/CO₂ mixture.

Isometric contraction protocol

LMB muscles were stimulated electrically by current passed between two platinum plate electrodes. The constant-current stimulation pulses were 0.5 ms in duration and their magnitude was adjusted to elicit a maximum twitch response. Optimum length (L_0) of each muscle was determined by adjusting muscle length until maximum twitch force was attained. To achieve a maximum isometric tetanic contraction, the muscle was stimulated with supramaximal intensity and frequency using pulses of alternating polarity. The protocol used to induce a force deficit consisted of 20 maximum isometric contractions, each lasting 1 second and separated by 1 minute. The

one minute rest period between contractions was necessary to eliminate fatigue, thereby ensuring that any decline in the force generating capability of the muscles during and after the 20 contractions was attributable to contraction-induced injury. To facilitate comparisons among groups of muscles that varied in mass, the absolute isometric force of each muscle during the contraction protocol was normalized to the maximum isometric force (P_o) produced by the muscle during the 20-contraction protocol.

Treatment groups

LMB muscles from WT mice were divided into two groups. One group was exposed to normal Tyrode solution and the other group to a nominally calcium-free Tyrode solution. LMB muscles from *mdx* mice were divided into 5 groups according to their treatment with: (i) P188, (ii) streptomycin, (iii) P188 and streptomycin, (iv) nominally calcium-free Tyrode, or (v) normal Tyrode. Streptomycin is an inhibitor of stretch-activated channels that reduces the magnitude of the contraction-induced force deficits in EDL muscles from *mdx* mice (32; 35). Experiments with streptomycin were included in the present study to validate the relatively novel LMB muscle preparation. Concentrations of P188 (Bayer, NJ) and streptomycin (Sigma, #S1277) in Tyrode solution were 1 mM and 200 μ M, respectively. For all treatments, muscles were allowed to incubate in the chamber for 15 minutes prior to commencement of the contraction protocol. Pilot experiments performed on WT muscles exposed to P188 (1 mM) or streptomycin (200 μ M) indicated that these compounds caused no decline in the P_o of the muscles when used at these concentrations. For nominally calcium-free experiments,

CaCl₂ was omitted from the Tyrode solution and MgCl₂ was increased to 2.3 mM to maintain the concentration of divalent cations.

Force deficits that arise from calcium-free experiments have two potential origins: a contraction-induced force deficit and an “environmental” force deficit caused by prolonged exposure of the muscle to a non-physiological environment. To separate the contraction-induced from the environmental force deficit, we assumed that the calcium-free environment had an effect that was equally deleterious to both WT and *mdx* muscles and consequently normalized the force responses of *mdx* muscles in calcium-free environments to those of WT muscles in the same calcium-free environments. At the end of the contraction protocol, isometric tetanic force of *mdx* muscles, expressed as a percentage of P₀, was divided by the isometric tetanic force of WT muscles, also expressed as a percentage of P₀. This procedure for the normalization of the data isolated the contraction-induced force deficits, allowing comparisons between the *mdx* muscles in calcium-free and normal environments.

Statistics

Data are presented as a mean value ± SEM. Statistical analyses were performed using analysis of variance (ANOVA) with the level of significance set *a priori* at P < 0.05. When significance was detected, the Holm-Sidak post hoc comparison was applied.

Results

Histology and isometric force production

LMB muscles were approximately 300 μm in diameter and consisted of 200 to 250 fibers (Fig 3.1A, B). Cross-sections from *mdx* muscles displayed typical dystrophic features (8) including areas of mononuclear cell infiltration and a population of fibers with central nuclei (Fig. 1C). The mean absolute P_o of untreated *mdx* muscles (10.8 ± 0.4 mN, $n=8$) was less than that of WT muscles (14.8 ± 0.9 mN, $n=6$). Treatment of *mdx* muscles with streptomycin, or P188, or with both streptomycin and P188 simultaneously, did not affect the absolute P_o (data not shown). In the nominally calcium-free Tyrode solution, the absolute P_o of both WT and *mdx* muscles decreased by $\sim 30\%$ to 10.8 ± 0.5 mN ($n=3$) and 7.2 ± 1.3 mN ($n=4$), respectively. This decrease in force is likely due to an impairment in the excitation-contraction coupling process caused by removal of calcium from the extracellular buffer (18).

Force production of WT and mdx muscles during the contraction protocol

Forces generated by LMB muscles from WT mice remained constant throughout the contraction protocol with no signs of fatigue or injury (Fig 3.2A & B). In contrast, untreated *mdx* muscles displayed a steady decline in force production as the protocol progressed (Fig 3.2B). Comparisons between *mdx* and WT muscles at individual contraction intervals revealed differences between the two genotypes for each contraction after the 7th. After a recovery period of 10 minutes, the magnitude of force was

unchanged, indicating that the force deficits observed in *mdx* LMB muscles were not caused by muscle fatigue but by contraction-induced injury (8).

Effects of P188 and streptomycin

At the end of the isometric contraction protocol, normalized force values were highest in the WT group and lowest in the untreated *mdx* group, at 98% and 69% of P_o , respectively (Fig 3.3). The *mdx* muscles in the P188+streptomycin group and in the calcium-free group generated normalized forces that were not different from muscles in the WT group (Fig 3.3). Treatment of *mdx* muscles with either P188 or streptomycin alone resulted in force values that were intermediate between the untreated *mdx* group and the WT group (Fig 3.3).

Discussion

The increased potential for permeability of the sarcolemma of dystrophic muscle fibers to extracellular calcium is likely to contribute to the increased susceptibility of dystrophic fibers to contraction-induced injury. In agreement with this hypothesis, we have shown previously that during a contraction protocol similar to the one used here, the contraction-induced mechanical failure of LMB muscles from the hindpaw of *mdx* mice was largely attributable to the influx of extracellular calcium into muscle fibers (11). Because of the direct relationship between increased intracellular calcium concentration and muscle dysfunction (3; 12; 31), therapeutic outcomes may be achieved through the identification and restriction of calcium influx pathways. In the present study, we confirm

that stretch-activated channels (SAC) (32; 35) are one such pathway and report the additional involvement of sarcolemmal lesions as contributors to contraction-induced force deficit in *mdx* skeletal muscles.

Previous studies have established P188 as a membrane-patching polymer that interacts directly with monolayers (33) and disrupted membranes (22). P188 is effective in stabilizing membranes and enhances the recovery of a variety of cell types from an array of injury-inducing protocols (7; 20; 25; 34). In the present study, P188 reduced the contraction-induced force deficit in *mdx* muscles by approximately 50% (Fig 3.3). A reduction in force deficit was also observed in *mdx* muscles that were exposed to a calcium-free environment. These results, coupled with a direct observation of calcium entry into dystrophic LMB muscle fibers during a similar contraction protocol (11), support the interpretation that the contraction protocol used in the present study results in sarcolemmal lesions that allow an influx of extracellular calcium, and that these entry pathways contribute significantly to the magnitude of the force deficit observed in *mdx* muscles. Despite the evidence of sarcolemmal lesions in *mdx* muscles, the mechanisms responsible for their formation remain uncertain. Given the vulnerability of the dystrophin-deficient sarcolemma (24; 27), lesions could have arisen from mechanical stress associated with contractile activity (23; 29), or alternatively, sarcolemmal lesions could result as a secondary consequence of Ca^{2+} entry into the muscle fibers (32). In this scenario, excessive influx of Ca^{2+} triggers the activity of lipid-damaging pathways (14) that induce lesions in the sarcolemma.

A treatment that combined both P188 and streptomycin produced only a marginal improvement over singly treated *mdx* muscles (Fig 3.3). The lack of a clear additive effect when P188 and streptomycin were used together suggests that, while both SAC and membrane lesions contribute to increased intracellular calcium, blockage of either pathway alone is sufficient to reduce the magnitude of the observed force deficit. Several potential explanations could account for this observation. One possibility is that the magnitude of calcium influx through either SAC or membrane lesions alone does not exceed the capacity of the muscle fibers to maintain intracellular calcium homeostasis. That is, endogenous calcium buffering, sequestration and extrusion pathways (4), coupled with a rapid membrane repair mechanism (2), might enable the muscle fibers to maintain normal levels of intracellular calcium as long as one of the calcium entry pathways is blocked. However, when calcium entry is occurring through both SAC and membrane lesions, the capacity of the calcium removal mechanisms might be exceeded, resulting in a calcium-induced force deficit. Another possibility is that the majority of sarcolemmal lesions repaired by P188 were a result of SAC activity. In this case, inhibition of SAC by streptomycin or repair of sarcolemmal lesions by P188 would be sufficient to rescue the muscle, and the combination of the two would not yield a pronounced improvement. Finally, we cannot exclude the possibility that P188 also acts as an inhibitor of SAC.

Using an isolated lumbrical muscle preparation, we have demonstrated for the first time that P188, a membrane sealing poloxamer, is effective in the reduction of contraction-induced force deficits in a whole *mdx* skeletal muscle. This observation supports the interpretation that the contractions cause sarcolemmal lesions that permit the

entry of extracellular calcium into muscle fibers. These results provide the basis for potential therapeutic strategies directed at membrane stabilization in dystrophin-deficient skeletal muscles.

Acknowledgements

The authors thank Carol Davis for assistance in data collection. This work was supported by grants AG000114, AG015434 and HL086790 from the National Institute of Health.

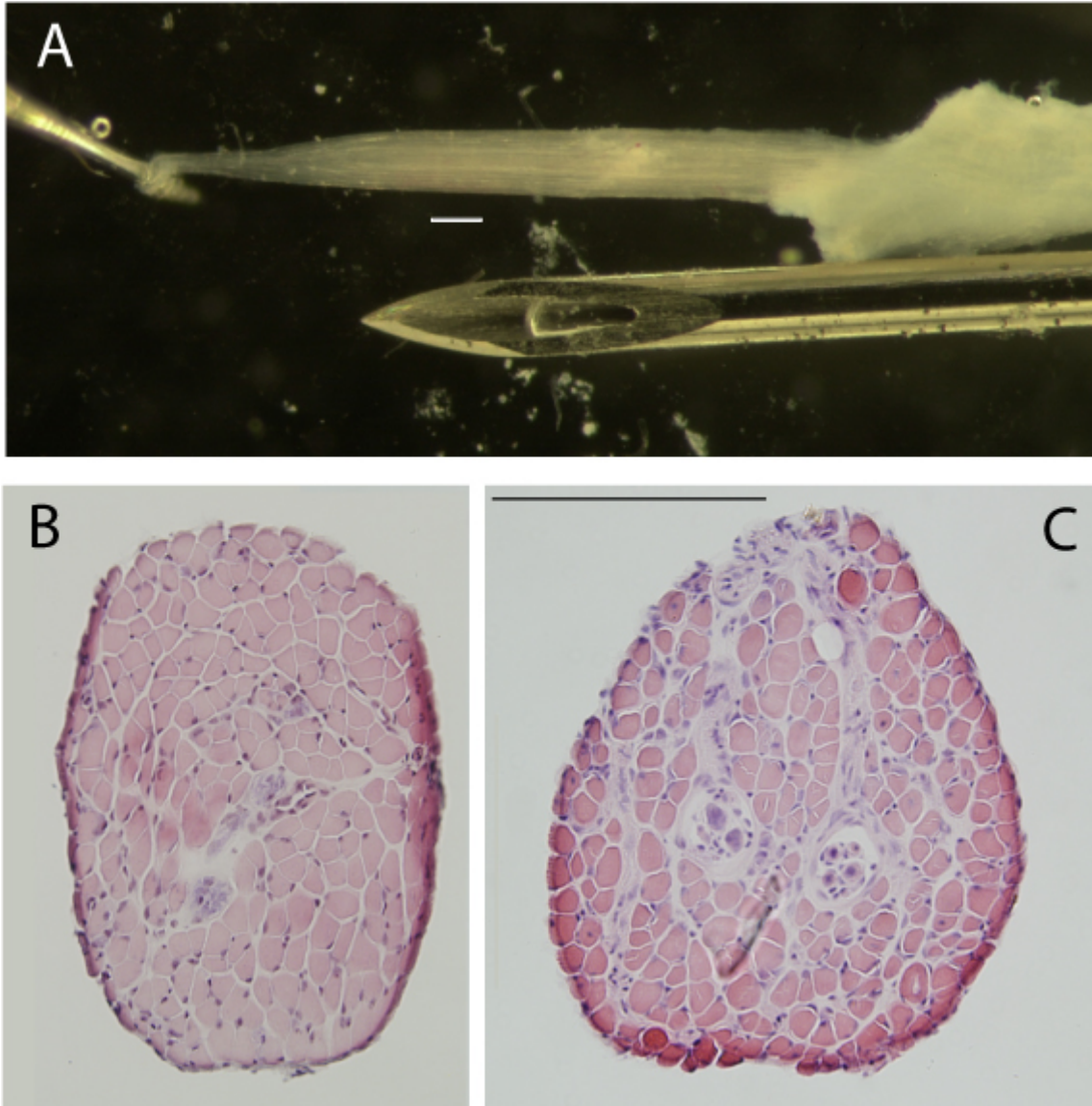


Fig 3.1. Lumbrical muscle from the 3rd digit of the forepaw of a mouse. (A) WT muscle is shown beside a 30G hypodermic needle. (B) Hematoxylin and eosin stained cross-section of a WT lumbrical muscle. Muscles typically consist of 200-250 fibers and are approximately 300 μm in diameter. (C) *mdx* muscle. Dystrophic features include presence of central nuclei and mononuclear cell infiltration. All scale bars are 200 μm and panels B and C share the same scale.

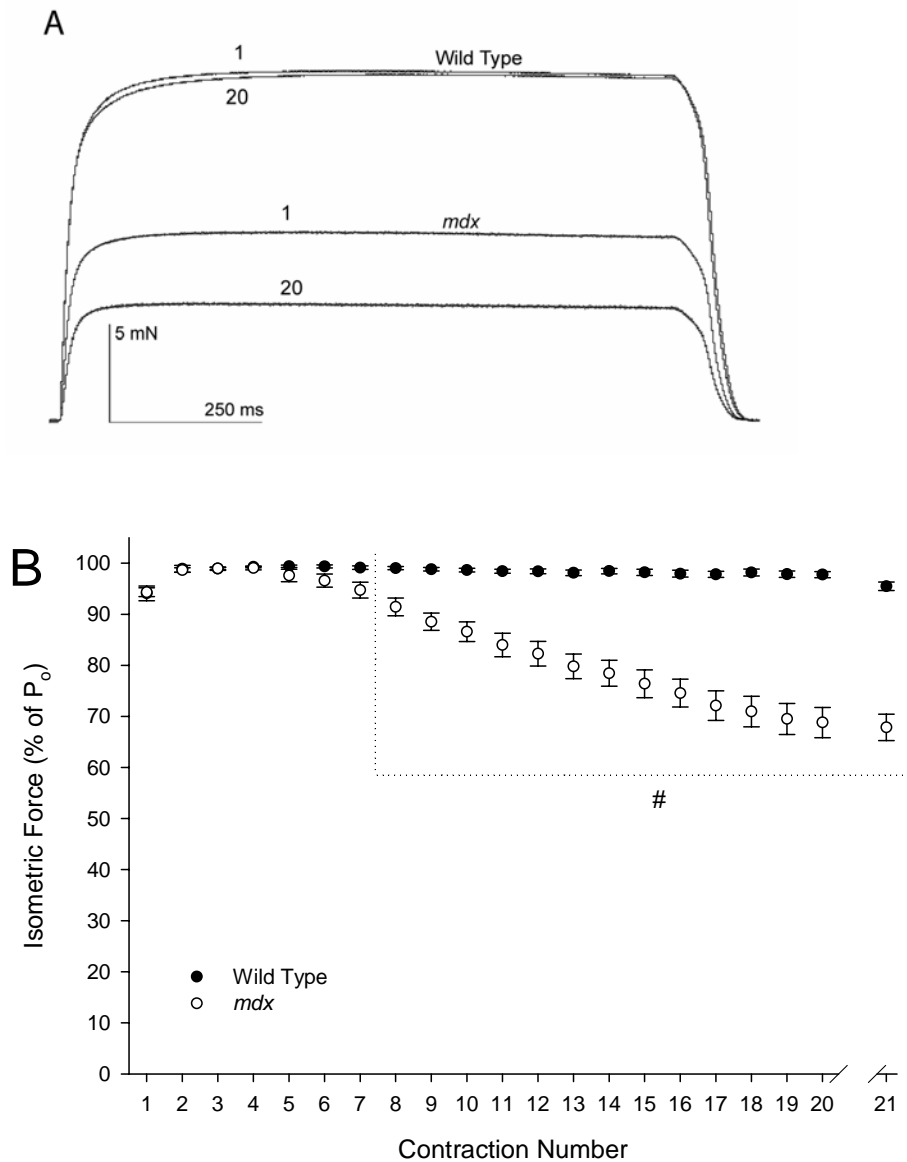


Fig 3.2. Force production of WT and *mdx* lumbrical muscles. (A) Example records of isometric force production. For clarity, only records of the first (1) and last (20) isometric contractions are shown. (B) Force production of WT (n=6) and *mdx* (n=8) lumbrical muscles during a protocol of 20 isometric contractions in normal Tyrode solution. Break in x-axis denotes a 10-minute rest period. A two-way ANOVA was performed to determine effects of dystrophin deficiency and contraction number on the force deficit. # indicates difference between WT and *mdx* muscles at matching time points ($P < 0.05$).

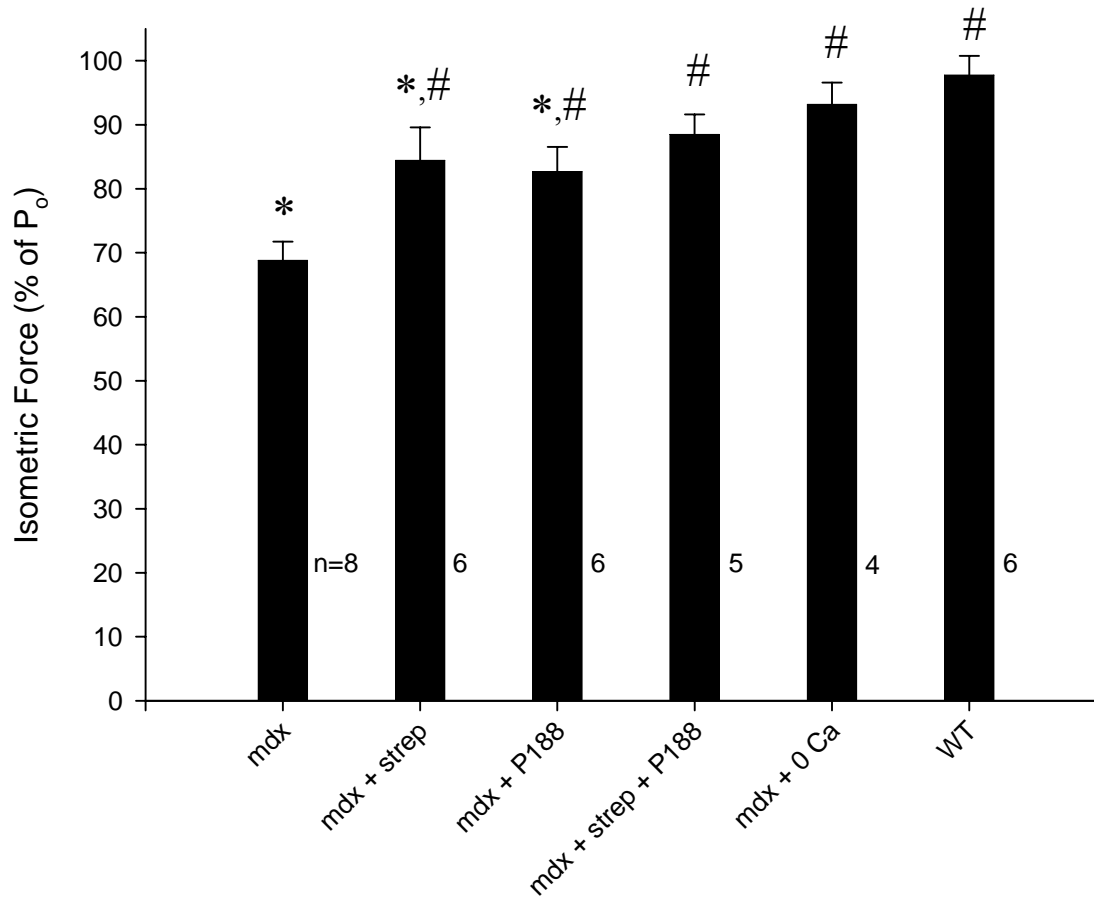


Fig 3.3. Force production of *mdx* and WT lumbrical muscles at the end of 20 isometric contractions. A one-way ANOVA was performed followed by 2 separate post hoc comparisons between groups. In the first comparison, all groups were compared against the untreated *mdx* group (Power > 0.8). In the second, all groups were compared against the WT group (Power > 0.8). * and # indicate difference from WT and untreated *mdx* group, respectively (P < 0.05).

References

1. **Archer JD, Vargas CC and Anderson JE.** Persistent and improved functional gain in mdx dystrophic mice after treatment with L-arginine and deflazacort. *FASEB J* 20: 738-740, 2006.
2. **Bansal D, Miyake K, Vogel SS, Groh S, Chen CC, Williamson R, McNeil PL and Campbell KP.** Defective membrane repair in dysferlin-deficient muscular dystrophy. *Nature* 423: 168-172, 2003.
3. **Belcastro AN, Shewchuk LD and Raj DA.** Exercise-induced muscle injury: a calpain hypothesis. *Mol Cell Biochem* 179: 135-145, 1998.
4. **Berchtold MW, Brinkmeier H and Muntener M.** Calcium ion in skeletal muscle: its crucial role for muscle function, plasticity, and disease. *Physiol Rev* 80: 1215-1265, 2000.
5. **Blake DJ, Weir A, Newey SE and Davies KE.** Function and genetics of dystrophin and dystrophin-related proteins in muscle. *Physiol Rev* 82: 291-329, 2002.

6. **Boittin FX, Petermann O, Hirn C, Mittaud P, Dorchies OM, Roulet E and Ruegg UT.** Ca²⁺-independent phospholipase A2 enhances store-operated Ca²⁺ entry in dystrophic skeletal muscle fibers. *J Cell Sci* 119: 3733-3742, 2006.
7. **Borgens RB, Bohnert D, Duerstock B, Spomar D and Lee RC.** Subcutaneous tri-block copolymer produces recovery from spinal cord injury. *J Neurosci Res* 76: 141-154, 2004.
8. **Brooks SV.** Rapid recovery following contraction-induced injury to *in situ* skeletal muscles in *mdx* mice. *J Muscle Res Cell Mot* 19: 179-187, 1998.
9. **Bulfield G, Siller WG, Wight PA and Moore KJ.** X chromosome-linked muscular dystrophy (*mdx*) in the mouse. *Proc Natl Acad Sci U S A* 81: 1189-1192, 1984.
10. **Burkholder TJ, Fingado B, Baron S and Lieber RL.** Relationship between muscle fiber types and sizes and muscle architectural properties in the mouse hindlimb. *J Morphol* 221: 177-190, 1994.
11. **Claffin DR and Brooks SV.** Direct observation of failing fibers in muscles of dystrophic mice provides mechanistic insight into muscular dystrophy. *Am J Physiol Cell Physiol* 294: C651-C658, 2008.

12. **Duncan CJ and Jackson MJ.** Different mechanisms mediate structural changes and intracellular enzyme efflux following damage to skeletal muscle. *J Cell Sci* 87 (Pt 1): 183-188, 1987.
13. **Fong PY, Turner PR, Denetclaw WF and Steinhardt RA.** Increased activity of calcium leak channels in myotubes of Duchenne human and mdx mouse origin. *Science* 250: 673-676, 1990.
14. **Gissel H.** The role of Ca²⁺ in muscle cell damage. *Ann N Y Acad Sci* 1066: 166-180, 2005.
15. **Head SI, Williams DA and Stephenson DG.** Abnormalities in structure and function of limb skeletal muscle fibres of dystrophic mdx mice. *Proc Biol Sci* 248: 163-169, 1992.
16. **Hill AV.** Diffusion of Oxygen Through Tissues. In: *Trails and Trials in Physiology*, Baltimore, MD: Williams & Wilkins, 1965, p. 208-241.
17. **Hoffman EP, Brown RH, Jr. and Kunkel LM.** Dystrophin: the protein product of the Duchenne muscular dystrophy locus. *Cell* 51: 919-928, 1987.

18. **Kotsias BA, Muchnik S and Obejero Paz CA.** Co^{2+} , low Ca^{2+} , and verapamil reduce mechanical activity in rat skeletal muscles. *Am J Physiol* 250: C40-C46, 1986.
19. **Kumar A, Khandelwal N, Malya R, Reid MB and Boriek AM.** Loss of dystrophin causes aberrant mechanotransduction in skeletal muscle fibers. *FASEB J* 18: 102-113, 2004.
20. **Lee RC, River LP, Pan FS, Ji L and Wollmann RL.** Surfactant-induced sealing of electropermeabilized skeletal muscle membranes in vivo. *Proc Natl Acad Sci U S A* 89: 4524-4528, 1992.
21. **Lynch GS, Hinkle RT, Chamberlain JS, Brooks SV and Faulkner JA.** Force and power output of fast and slow skeletal muscles from mdx mice 6-28 months old. *J Physiol* 535: 591-600, 2001.
22. **Maskarinec SA, Wu G and Lee KY.** Membrane sealing by polymers. *Ann N Y Acad Sci* 1066: 310-320, 2006.
23. **McNeil PL and Khakee R.** Disruptions of muscle fiber plasma membranes. Role in exercise-induced damage. *Am J Pathol* 140: 1097-1109, 1992.

24. **Menke A and Jockusch H.** Decreased osmotic stability of dystrophin-less muscle cells from the mdx mouse. *Nature* 349: 69-71, 1991.
25. **Merchant FA, Holmes WH, Capelli-Schellpfeffer M, Lee RC and Toner M.** Poloxamer 188 enhances functional recovery of lethally heat-shocked fibroblasts. *J Surg Res* 74: 131-140, 1998.
26. **Ohlendieck K and Campbell KP.** Dystrophin-associated proteins are greatly reduced in skeletal muscle from mdx mice. *J Cell Biol* 115: 1685-1694, 1991.
27. **Pasternak C, Wong S and Elson EL.** Mechanical function of dystrophin in muscle cells. *J Cell Biol* 128: 355-361, 1995.
28. **Petrof BJ.** Molecular pathophysiology of myofiber injury in deficiencies of the dystrophin-glycoprotein complex. *Am J Phys Med Rehabil* 81: S162-S174, 2002.
29. **Petrof BJ, Shrager JB, Stedman HH, Kelly AM and Sweeney HL.** Dystrophin protects the sarcolemma from stresses developed during muscle contraction. *Proc Natl Acad Sci U S A* 90: 3710-3714, 1993.
30. **Straub V, Rafael JA, Chamberlain JS and Campbell KP.** Animal models for muscular dystrophy show different patterns of sarcolemmal disruption. *J Cell Biol* 139: 375-385, 1997.

31. **Verburg E, Murphy RM, Stephenson DG and Lamb GD.** Disruption of excitation-contraction coupling and titin by endogenous Ca²⁺-activated proteases in toad muscle fibres. *J Physiol* 564: 775-790, 2005.

32. **Whitehead NP, Streamer M, Lusambili LI, Sachs F and Allen DG.** Streptomycin reduces stretch-induced membrane permeability in muscles from mdx mice. *Neuromuscul Disord* 16: 845-854, 2006.

33. **Wu G, Majewski J, Ege C, Kjaer K, Weygand MJ and Lee KY.** Interaction between lipid monolayers and poloxamer 188: an X-ray reflectivity and diffraction study. *Biophys J* 89: 3159-3173, 2005.

34. **Yasuda S, Townsend D, Michele DE, Favre EG, Day SM and Metzger JM.** Dystrophic heart failure blocked by membrane sealant poloxamer. *Nature* 436: 1025-1029, 2005.

35. **Yeung EW, Whitehead NP, Suchyna TM, Gottlieb PA, Sachs F and Allen DG.** Effects of stretch-activated channel blockers on [Ca²⁺]_i and muscle damage in the mdx mouse. *J Physiol* 562: 367-380, 2005.

Chapter 4

Fluorescent indicators reveal no evidence of sarcolemmal lesions in whole skeletal muscles during lengthening contractions

Abstract

After a protocol of lengthening contractions, leakage of cytosolic enzymes and influx of membrane-impermeable dyes have been used as evidence of lesions in the sarcolemma. The causes of these contraction-induced lesions cannot be established through results from enzyme leakage and dye uptake assays because of the limited temporal resolution that these techniques provide. In the present study, we describe the use of two fluorescence-based methods capable of reporting membrane lesions with high temporal resolution. Utilizing these improved assays, we sought to determine whether mechanical stress alone is sufficient to produce contraction-induced sarcolemmal lesions. Fluorescent dyes Fluo-4 and FM1-43 were applied to a very small whole skeletal muscle from the forepaw of the mouse and the fluorescence responses of both dyes were monitored during an acute protocol of 15 severe lengthening contractions. Analysis of fluorescence responses throughout the contraction protocol revealed no evidence of mechanically-induced lesions in the sarcolemma. Similar results were obtained from muscles that had an impaired membrane-repair mechanism. These results indicate that mechanical stresses associated with the lengthening contraction protocol, while severe

enough to cause a 30% force deficit, did not produce sarcolemmal lesions in the fibres of an intact skeletal muscle. This finding supports the idea that contraction-induced sarcolemmal lesions arise from a combination of biochemical as well as mechanical stressors, and that mechanical stress is not the direct cause of the contraction-induced lesions reported by dye-influx and/or enzyme-efflux assays.

Introduction

Daily activity and physical exercise subject muscles to considerable mechanical stress and changes in length (11). Muscles exposed to lengthening contractions frequently sustain force deficits that are associated with contraction-induced injury (9; 10). Immediately after an injurious contraction protocol, muscles exhibit disruptions to force generating structures (10; 26), a reduction in function of the excitation-contraction coupling system (36; 39), and an increase in proteolytic activity (4). Sarcolemmal lesions are also associated with contraction-induced injury, inferred from the movement of bulky, membrane impermeable dyes and enzymes across the membrane (1; 12; 27). The contraction-induced lesions are thought to occur as a direct result of mechanical stress generated during contractile activity (1; 27; 33). The evidence for this interpretation is weakened by the low temporal resolution associated with dye-uptake and enzyme-efflux assays, which typically require substantial periods of contractile activity or incubation (~60-90min) (27; 34; 38). Prolonged contractile activity and/or incubation times (4; 15; 42) result in an increase in the activity of proteases, phospholipases and reactive oxygen species, increasing the likelihood of their contribution to sarcolemmal disruptions (17).

Consequently, the lesions that are reported by these assays may be partially attributable to biochemical stressors. The purpose of the present study was to determine the direct effect of mechanical stress on contraction-induced membrane lesions.

To minimize contributions from biochemical stressors, we utilized a short experimental protocol that consisted of 15 severe lengthening contractions performed over a period of 15 min. As traditional dye/enzyme membrane permeability assays do not allow the detection of membrane lesions over brief time periods, we employed alternative detection assays based on the fluorescent indicators Fluo-4 and FM1-43. Both indicators have been used previously to detect membrane breaches (2; 3; 22; 28). The fluorescent indicators were applied to a very small whole muscle preparation, the lumbrical muscle, obtained from the forepaw of the mouse (32). The lumbrical muscles were subjected to the protocol of lengthening contractions and the fluorescence emissions from both Fluo-4 and FM1-43 were monitored. To amplify any effects of membrane lesions, the same contraction protocol was also performed on muscles that lack dysferlin, a protein that augments the membrane repair process (3; 24; 25). We hypothesized that during a protocol of lengthening contractions, fluorescence from both Fluo-4 and FM1-43 would increase, reflecting the presence of membrane lesions, and that the fluorescence increases would be greater in dysferlin-null muscle.

Methods

Specific-pathogen-free male wild-type (WT) C57BL/6 and dysferlin null mice (A/J, stock #000686) mice 8-12 months of age were obtained from the Jackson

Laboratory (Bar Harbor, ME). A/J mice exhibit a complete loss of dysferlin and display symptoms of progressive muscular dystrophy that includes elevated serum CK levels, myofibre degeneration and regeneration and muscle inflammation (20). References to muscles from A/J and wild-type mice will hereafter be termed *dysf*-null and WT muscles, respectively. Mice were housed in a specific-pathogen-free barrier facility at the University of Michigan. All experimental procedures were approved by the University of Michigan Committee on the Use and Care of Animals and in accordance with the *Guide for the Care and Use of Laboratory Animals* [DHHS Publication No. 85–23 (NIH), Revised 1985, Office of Science and Health Reports, Bethesda, MD 20892].

Operative Procedure

Mice were anesthetized with an intraperitoneal injection of Avertin (tribromoethanol 400mg/kg). Supplemental doses of Avertin were administered as required to keep the mouse unresponsive to tactile stimuli. The front paws were removed and the lumbrical (LMB) muscles dissected free from the third digit. The benefits of using LMB muscles as models to study contraction-induced injury have been discussed previously (13; 32). The mice were subsequently euthanized by an overdose of Avertin followed by a thoracotomy. Dissections were performed in a chilled bathing solution (approx. 8°C), composition (in mM): 137 NaCl, 11.9 NaHCO₃, 5.0 KCl, 1.8 CaCl₂, 0.5 MgCl₂, 0.4 NaH₂PO₄. The isolated LMB muscle was mounted horizontally in a custom-fabricated chamber with the distal tendon attached to a force transducer (Aurora Scientific, Inc., modified Model 400A) and the proximal tendon to a servomotor (Aurora

Scientific, Inc., Model 318B). The ties were composed of 10-0 monofilament nylon suture. Bath temperature was maintained at 25°C and the chamber was perfused continuously with Tyrode solution, except during FM1-43 experiments where, instead of perfusion, the entire bath was changed every 5 minutes. The composition of the Tyrode solution was (in mM): 121 NaCl, 24 NaHCO₃, 5.0 KCl, 1.8 CaCl₂, 0.5 MgCl₂, 0.4 NaH₂PO₄. For nominally calcium-free experiments, CaCl₂ was omitted from the Tyrode solution and MgCl₂ was increased to 2.3 mM to maintain the concentration of divalent cations. A pH of 7.3 was maintained by bubbling with a 95%/5% O₂/CO₂ mixture.

Protocol for inducing injury

Muscles were stimulated electrically by current passed between two platinum plate electrodes. The constant-current stimulation pulses were 0.5 ms in duration and their magnitude was adjusted to elicit a maximum twitch response. Optimum length (L_0) of each muscle was determined by adjusting muscle length until maximum twitch force was attained. LMB muscles are sufficiently small that individual fibres can be discerned, allowing the length of muscle fibres (L_f) to be determined visually when the muscle was at L_0 . To achieve a maximum isometric tetanic contraction, the muscle was stimulated with supramaximal intensity and frequency using pulses of alternating polarity. The stimulation duration for each lengthening contraction was 700 ms and a stretch at 30% L_f was applied 300 ms after the start of stimulation. The muscle was lengthened at 0.75 L_f/s , causing the peak of the stretch to coincide with the end of tetanic stimulation, 400 ms after the initiation of the stretch. The lengthening contractions were applied at 1 minute

intervals and the protocol consisted of 15 such contractions. We have shown previously that LMB muscles subjected to a similar protocol of isometric contractions do not exhibit fatigue or deterioration (32). To facilitate comparisons among groups of muscles that varied in mass, the absolute isometric force of each muscle during the contraction protocol was normalized to the maximum isometric force (P_o) produced by the muscle during the 15-contraction protocol.

FM1-43 and Fluo-4 as indicators of membrane breaches

Both FM1-43 and Fluo-4 have been demonstrated to be reliable indicators of membrane breaches, albeit through distinct, independent mechanisms (14; 37). FM1-43 is a membrane-impermeable dye that fluoresces when partitioned into membranes (14). In the presence of membrane breaches, the fluorescence intensity of FM1-43 increases many-fold as the dye enters the cell and rapidly partitions into intracellular membrane surfaces (3; 28). Fluo-4 is a highly sensitive Ca^{2+} indicator ($K_d \sim 345\text{nm}$) (16) that exhibits a ~ 100 -fold enhancement in fluorescence upon binding with Ca^{2+} (19). Cells loaded with Fluo indicators respond dramatically to breaches in the membrane (2; 22), as Ca^{2+} from the extracellular space enters the cell, driven by a concentration gradient of 18,000:1 (40).

Measurements of fluorescence from FM1-43 and Fluo-4

A buffer containing FM1-43 (2.5 μM) was prepared by dissolving the dye in freshly-oxygenated Tyrodes solution. The prohibitive cost of FM1-43 rendered its

continuous perfusion unfeasible. Instead, the FM1-43 buffer was replaced every 5 minutes with a new preparation from freshly-oxygenated Tyrodes solution. Prior to the lengthening contraction protocol, fluorescence measurements were made to ensure that muscle had achieved equilibrium with the FM1-43 buffer. Fluorescence was elicited by epi-illumination from a 75 W xenon lamp and detected using a photomultiplier tube (Photon Technology International, model R1527 PMT). The wavelengths for excitation were centred at 479 nm (bandwidth 2 nm), selected using a diffraction grating monochromator (PTI, model Deltascan 4000). The emitted fluorescence passed through a longpass filter (520 nm) before reaching the photomultiplier tube. During the lengthening contraction protocol, fluorescence measurements were taken 30 s after each contraction at a sample rate of 100 measurements per second for 5 s. The median of the 500 measurements was taken to be the fluorescence value after each lengthening contraction.

For the Ca^{2+} -sensing experiments, LMB muscles were loaded simultaneously with Fluo-4 and Fura-PE3 (Teflabs, Austin, TX). Both dyes were loaded in membrane-permeant acetoxymethyl ester (AM) forms at $15\mu\text{M}$ and 25°C for 30 min. Pluronic F-127 (0.01 % w/v; Molecular Probes) was used as a dispersing agent. The combined use of Fura-PE3 and Fluo-4 was employed because the fluorescence measured from non-ratioable dyes, such as Fluo-4, is susceptible to fluctuations not related to $[\text{Ca}^{2+}]$, such as those caused by dye leakage and loading non-uniformity. In contrast, dual-wavelength excitation of ratioable indicators such as Fura-PE3 produces a response that is much less sensitive to fluctuations in dye concentration (30; 31). Fura-PE3, however, becomes less reliable upon commencement of the contraction protocol, as its excitation spectrum

overlaps that of NADH (7), an intracellular coenzyme that fluctuates in concentration during muscle activity (23). To overcome the inherent limitations of Fluo-4 and Fura-PE3, a linear scaling algorithm was developed that used ratiometric measurements of Fura-PE3 made during periods of muscle inactivity, to transform the signal from Fluo-4 into a pseudo-ratio signal. This was done by adjusting the Fluo-4 signal using two ratiometric measurements of Fura-PE3, one taken before the lengthening contraction protocol and the other 5 minutes after (see Fig 4.1).

Fluorescence of Fura-PE3 was achieved by exciting the muscle with two alternating wavelengths set by diffraction grating monochromators centred at 375 and 340 nm (bandwidth 4 nm). The emitted fluorescence was passed through a 510 nm bandpass filter (bandwidth 40 nm) and fluorescence was measured at a rate of 10 wavelength pairs per second. For Fluo-4 measurements, an excitation wavelength centred at 493 nm (bandwidth 4 nm) was used and the emitted fluorescence passed through a 535 nm bandpass filter (bandwidth 40 nm) and was sampled at 100 measurements per second. The Fluo-4 signal was then processed using the standard median filter in MATLAB[®] (Mathworks, Natick, MA) set to a window size of 17 data points. To quantify the fluorescence intensity of Fluo-4 after each lengthening contraction, the pseudo-ratio signal from Fluo-4 was integrated over a period of 59 s, starting 300 ms after cessation of electrical stimulation (see Fig 4.1). The 300 ms delay was incorporated to minimize movement-associated artefacts in the fluorescence response and to allow time for both the $[Ca^{2+}]$ and rate of change of $[Ca^{2+}]$ to fall to levels that could be reported by Fluo-4 with minimal distortion (16).

Statistics

Data are presented as a mean value \pm SEM. Statistical analyses were performed using analysis of variance (ANOVA) with the level of significance set *a priori* at $P < 0.05$. When significance was detected, the Holm-Sidak post hoc comparison was applied.

Results

Force production

The absolute P_o of *dysf*-null muscles (10.9 ± 0.8 mN, $n=5$) was less than that of WT muscles (14.7 ± 0.9 mN, $n=7$). When subjected to a protocol of 15 lengthening contractions, WT and *dysf*-null muscles exhibited final force deficits of 30 ± 4 % and 23 ± 3 %, respectively (Fig 4.2). The magnitude of force deficit was unchanged after a 10 min recovery period (data not shown), indicating that the force deficits observed were not influenced by muscle fatigue, but rather were due to contraction-induced injury (8). Comparisons between *dysf*-null and WT muscles at individual contraction intervals revealed differences between the two genotypes for each response after the 9th contraction (Fig 4.2).

FM1-43 intensity during lengthening contraction protocol.

Throughout the lengthening contraction protocol, the fluorescence intensity of FM1-43 in *dysf*-null muscles was not different from WT muscles (Fig 4.3). To serve as a positive control, lengthening contractions were also carried out in the presence of

phospholipase A₂ (15µg/ml, Sigma), a myotoxin found in bee venom that disrupts the integrity of the sarcolemma (18). Muscles exposed to phospholipase A₂ exhibited an increase in FM1-43 signal intensity throughout the progression of the lengthening contraction protocol (Fig 4.3).

Concentration of intracellular calcium ($[Ca^{2+}]_i$) from measurements of Fluo-4

The time-integral of the pseudo-ratio signal of Fluo-4 after each lengthening contraction (see Methods) yielded the intercontraction $[Ca^{2+}]_i$, hereafter abbreviated as $[Ca^{2+}]_{int}$. In both WT and *dysf*-null muscles, the $[Ca^{2+}]_{int}$ remained constant throughout the contraction protocol (Fig 4.4). Although $[Ca^{2+}]_{int}$ was unchanged in both mouse models, the $[Ca^{2+}]_{int}$ was consistently greater in *dysf*-null muscles (Fig 4.4). The $[Ca^{2+}]_{int}$ of *dysf*-null muscle was unaltered by the removal of Ca²⁺ from the extracellular buffer (Fig 4.4).

Discussion

After contractile activity, dye-influx and enzyme-efflux assays indicate an increase in membrane permeability of skeletal muscles under both *in vivo* (6; 27) and *in vitro* (38) conditions. The increase in membrane permeability reported by these assays arises from either mechanical stress, biochemical processes (17), or a combination the two. Typical dye-influx and enzyme-efflux assays require substantial periods of contractile activity or incubation with the dye (27; 34; 38). Consequently, these tests cannot differentiate between membrane breaches caused directly by mechanical stress

and those caused by biochemical processes. We subjected whole skeletal muscles from both WT and *dysf*-null mice to a brief protocol of injury-inducing lengthening contractions and, using two independent fluorescence-based detection assays, monitored the muscles continuously for evidence of mechanically-induced membrane lesions. Contrary to our hypothesis, we found no evidence that membrane breaches were being formed during the protocol of lengthening contractions.

Force deficits following the lengthening contraction protocol

Compared with isometric contractions or passive stretches, lengthening contractions generate the greatest mechanical stress and ultrastructural damage to muscle (26) and are therefore most suitable for studying mechanically-induced lesions in the membrane. Our lengthening contraction protocol was deliberately limited to 15 minutes with ample time for recovery between contractions. These parameters ensured that changes in membrane permeability, if detected, would be attributable directly to mechanical stress and not membrane-targeting biochemical processes that are augmented by fatiguing protocols or extended incubation (4; 15; 42). The 30% force deficit elicited by our contraction protocol is either similar to (12), or greater than (38), the force deficits reported in traditional membrane permeability assays in which enzyme-efflux was detected. The similarity in force deficits indicates that absence of membrane lesions in the present study cannot be explained simply by inadequate levels of mechanical stress.

FM1-43 and Fluo-4 yield no evidence of membrane lesions

FM1-43 is membrane-impermeant indicator that has been used previously to detect disruptions of the plasma membrane (3; 28). Bansal *et. al.* demonstrated that a single laser-induced lesion in the sarcolemma of WT muscle fibres elicits a substantial increase in the fluorescence intensity of FM1-43 and that the increase is even more pronounced in *dysf*-null muscle fibres (3). When subjected to the present protocol of lengthening contractions, neither WT nor *dysf*-null muscles exhibited an increase FM1-43 fluorescence (Fig 4.3), suggesting that contraction-induced membrane lesions were not present in either mouse model. In contrast, WT muscles exposed to phospholipase A₂ sustained disruptions to the membrane that were clearly reported by FM1-43 (Fig 4.3).

To obtain an additional, independent assessment of sarcolemmal integrity, a further series of experiments was performed utilizing Fluo-4, a sensitive Ca²⁺ indicator used routinely to measure [Ca²⁺]_i (21; 41). Fluo indicators have been adapted successfully for the detection of membrane lesions, as they report effectively the increase in [Ca²⁺]_i that results from membrane breaches (2; 22). In the present study, the [Ca²⁺]_{int} of both WT and *dysf*-null muscles remained constant throughout the lengthening contraction protocol (Fig 4.4), providing additional support for the conclusion that membrane lesions were not being formed as a direct consequence of high stress levels. Although [Ca²⁺]_{int} remained unchanged in both mouse models, the [Ca²⁺]_{int} was consistently greater in *dysf*-null muscles (Fig 4.4). The larger [Ca²⁺]_{int} observed in *dysf*-null muscle could be due to a less rapid removal of cytosolic Ca²⁺ by endogenous Ca²⁺ sequestering systems, or by a steady leakage of extracellular Ca²⁺ into the muscle fibres. To distinguish between these

two possibilities, lengthening contractions were performed on *dysf*-null muscles in a Ca^{2+} -free buffer. The $[\text{Ca}^{2+}]_{\text{int}}$ response was unaltered by the removal of Ca^{2+} from the bathing medium, indicating that the elevated $[\text{Ca}^{2+}]_{\text{int}}$ observed in *dysf*-null muscle was not attributable to entry of extracellular Ca^{2+} . We postulate that the elevated $[\text{Ca}^{2+}]_{\text{int}}$ observed in *dysf*-null results from genetic differences between the BL/6 and A/J mice (29), or alternatively, that the lack of dysferlin affects the post-activation Ca^{2+} sequestering processes in the A/J mice.

Role of mechanical stress in the formation of sarcolemmal lesions

Despite sustaining a post-protocol force deficit of ~30%, LMB muscles did not show any evidence of sarcolemmal lesions, suggesting that the sarcolemma was able to tolerate mechanical stress relatively well. The resilience of the sarcolemma to mechanical stress may be attributable to protective mechanisms such as lateral force transmission pathways (5) and indentations (35) in the membrane that help to minimize damage to the membrane during contractile activity. These protective mechanisms, however, become inadequate during prolonged contractile activity or incubation, as evidenced by the movement of membrane-impermeant dyes and enzymes across the sarcolemma (1; 12; 27). These sarcolemmal breaches occurred despite inducing force deficits that were only half as large as those of the present study (1; 12). These observations, coupled with the fact that deleterious membrane-targeting processes are augmented by prolonged contractile activity or incubation (4; 15; 42), suggest that membrane-targeting processes

such as phospholipases, calpains and ROS may play a more significant role in the formation of contraction-induced sarcolemmal lesions than previously anticipated.

Our results suggest that mechanical stress alone, when applied within physiological boundaries, is insufficient to elicit sarcolemmal lesions in a whole skeletal muscle. Instead, sarcolemmal lesions are likely to be formed through a combination of biochemical and mechanical stressors. The present study offers new insights into the relationship between mechanical stress and sarcolemmal disruption, contributing to the understanding of the initial events that occur in contraction-induced injury.

Acknowledgements

This work was supported by grants AG 000114, AG 20591 and AG 015434 from the National Institute on Aging

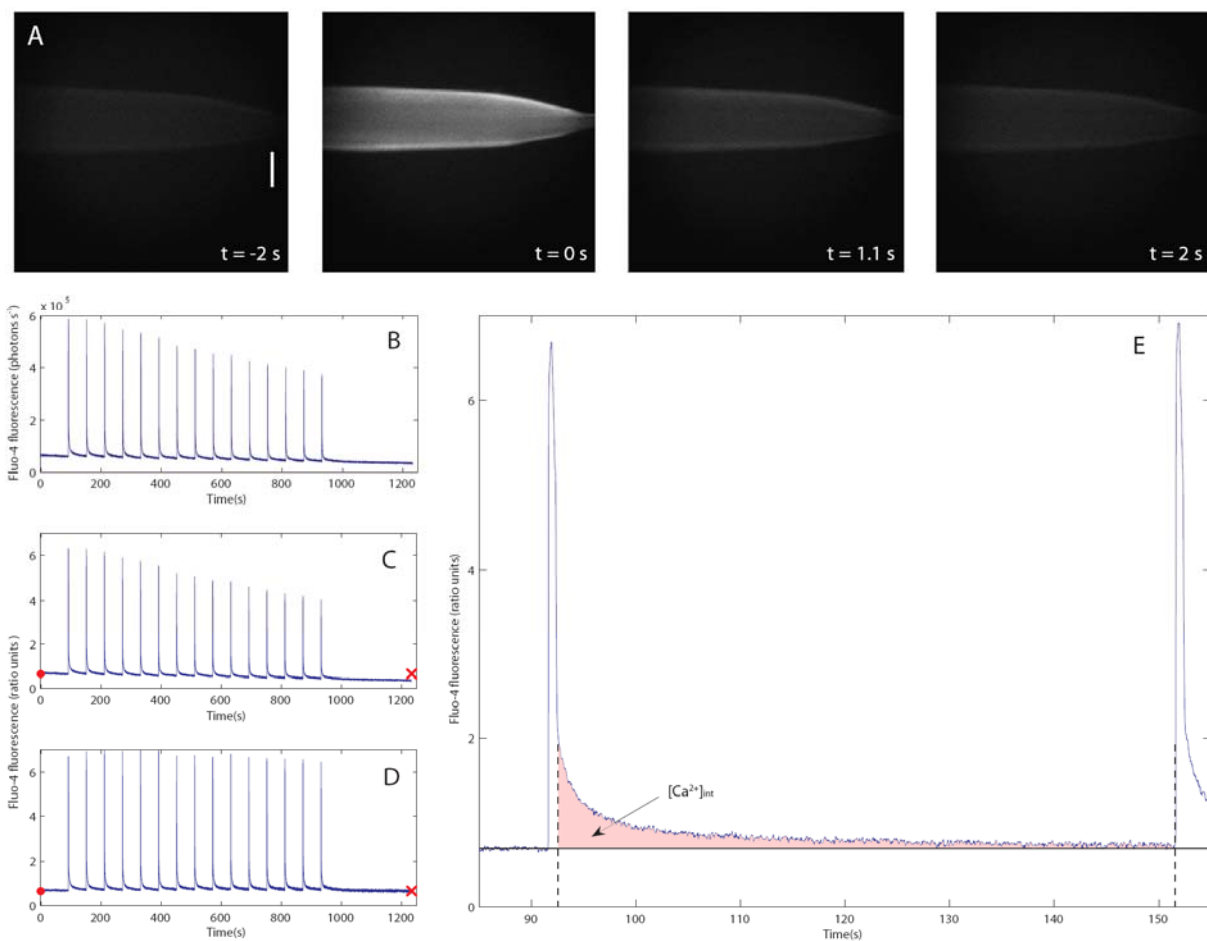


Fig 4.1. Measurements from ratioable indicator Fura-PE3 transform Fluo-4 fluorescence into a pseudo-ratio signal. The motivation for generating a pseudo-ratio signal is described in METHODS. (A) LMB muscle loaded with Fluo-4/Fura-PE3 and subjected to a single lengthening contraction. Images were acquired by an electron-multiplying CCD camera (Photometrics[®] QuantEM:512SC) and used solely for visualization purposes. (B) Typical experimental record of Fluo-4 fluorescence intensity depicting a gradual decline due to Ca^{2+} -independent factors such as dye leakage or compartmentalization into intracellular organelles. (C) The Fluo-4 signal is anchored to an initial ratio measurement from Fura-PE3 (●). Note that the gradual decline in Fluo-4 intensity remains uncorrected. (D) The Fluo-4 signal is further transformed using a Fura-PE3 ratio measurement (×) taken 5 min after the contraction protocol. This was done by multiplying the entire Fluo-4 signal with a linear scaling array. The result is a transformation of the Fluo-4 signal into pseudo-ratio signal. Note the correction in the decline of Fluo-4 intensity. (E) Close-up of 1st peak depicting the area used to quantify intracellular $[\text{Ca}^{2+}]_{\text{int}}$. The area (shaded) was obtained by computing the time-integral bounded by the dashed and solid lines.

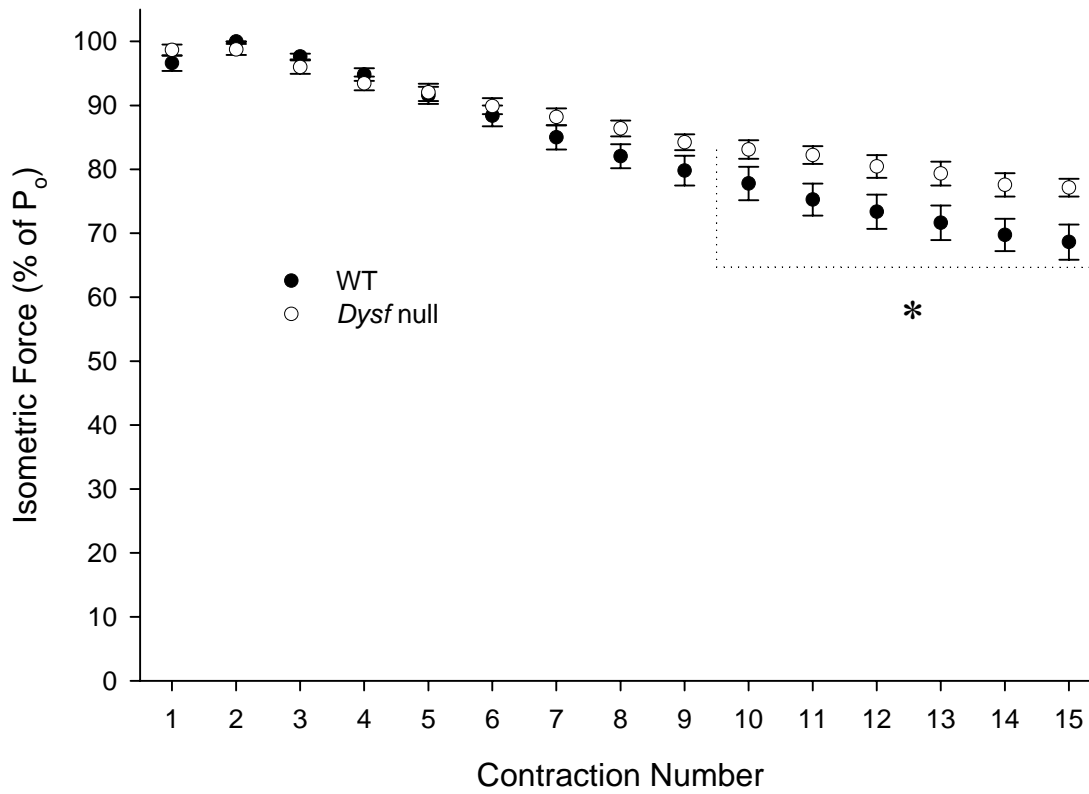


Fig 4.2. Force production of WT and *dysf*-null lumbrical muscles. Gradual decline in force production of muscles from both mouse models during a protocol of 15 lengthening contractions. * indicates difference between WT and *dysf*-null muscles at matching time points ($P < 0.05$).

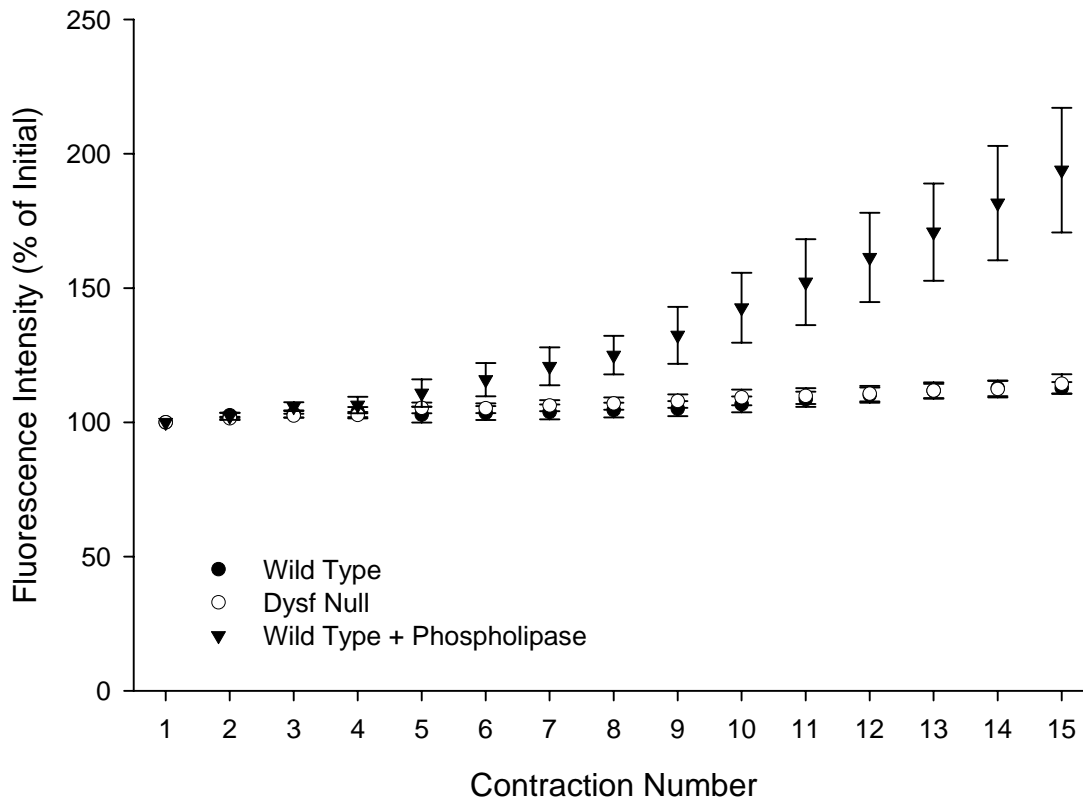


Fig 4.3. Normalized fluorescence intensities of FM1-43 during progression of lengthening contraction protocol. Fluorescence intensity of FM1-43 was captured 30s after each lengthening contraction in WT and *dysf*-null muscle. ANOVA revealed no differences between genotypes. As a positive control, the lengthening contraction protocol was also carried out in the presence of phospholipase A₂, which causes disruptions in the membrane.

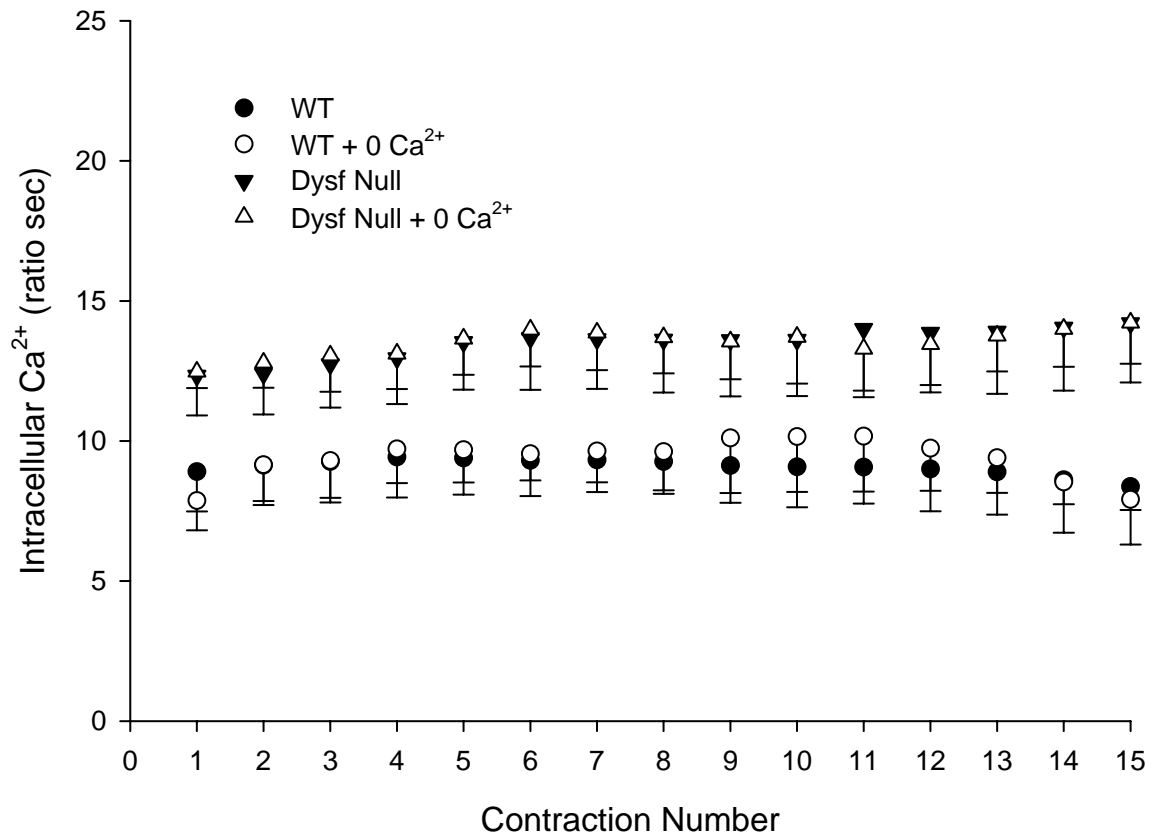


Fig 4.4. Intercontraction $[Ca^{2+}]_i$ ($[Ca^{2+}]_{int}$) during progression of lengthening contraction protocol. Responses were quantified by computing the time-integral of the pseudo-ratio signal from Fluo-4 (see Fig 4.1). Data from experiments with calcium omitted from the buffer are denoted as “0 Ca²⁺”. A three-way ANOVA was performed to determine effects of (1) dysferlin deficiency, (2) contraction number and (3) calcium in extracellular buffer on the $[Ca^{2+}]_{int}$. Only dysferlin deficiency affected $[Ca^{2+}]_{int}$ ($P < 0.05$).

References

1. **Armstrong RB, Ogilvie RW and Schwane JA.** Eccentric exercise-induced injury to rat skeletal muscle. *J Appl Physiol* 54: 80-93, 1983.
2. **Baldwin TJ, Ward W, Aitken A, Knutton S and Williams PH.** Elevation of intracellular free calcium levels in HEp-2 cells infected with enteropathogenic *Escherichia coli*. *Infect Immun* 59: 1599-1604, 1991.
3. **Bansal D, Miyake K, Vogel SS, Groh S, Chen CC, Williamson R, McNeil PL and Campbell KP.** Defective membrane repair in dysferlin-deficient muscular dystrophy. *Nature* 423: 168-172, 2003.
4. **Belcastro AN.** Skeletal muscle calcium-activated neutral protease (calpain) with exercise. *J Appl Physiol* 74: 1381-1386, 1993.
5. **Bloch RJ, Capetanaki Y, O'Neill A, Reed P, Williams MW, Resneck WG, Porter NC and Ursitti JA.** Costameres: repeating structures at the sarcolemma of skeletal muscle. *Clin Orthop Relat Res* S203-S210, 2002.

6. **Boppart MD, Burkin DJ and Kaufman SJ.** Alpha7beta1-integrin regulates mechanotransduction and prevents skeletal muscle injury. *Am J Physiol Cell Physiol* 290: C1660-C1665, 2006.
7. **Brachmanski M, Gebhard MM and Nobiling R.** Separation of fluorescence signals from Ca²⁺ and NADH during cardioplegic arrest and cardiac ischemia. *Cell Calcium* 35: 381-391, 2004.
8. **Brooks SV.** Rapid recovery following contraction-induced injury to *in situ* skeletal muscles in *mdx* mice. *J Muscle Res Cell Mot* 19: 179-187, 1998.
9. **Brooks SV and Faulkner JA.** Severity of contraction-induced injury is affected by velocity only during stretches of large strain. *J Appl Physiol* 91: 661-666, 2001.
10. **Brooks SV, Zerba E and Faulkner JA.** Injury to muscle fibres after single stretches of passive and maximally stimulated muscles in mice. *J Physiol* 488 (Pt 2): 459-469, 1995.
11. **Burkholder TJ and Lieber RL.** Sarcomere length operating range of vertebrate muscles during movement. *J Exp Biol* 204: 1529-1536, 2001.

12. **Carter GT, Kikuchi N, Abresch RT, Walsh SA, Horasek SJ and Fowler WM, Jr.** Effects of exhaustive concentric and eccentric exercise on murine skeletal muscle. *Arch Phys Med Rehabil* 75: 555-559, 1994.
13. **Clafin DR and Brooks SV.** Direct observation of failing fibers in muscles of dystrophic mice provides mechanistic insight into muscular dystrophy. *Am J Physiol Cell Physiol* 294: C651-C658, 2008.
14. **Cochilla AJ, Angleson JK and Betz WJ.** Monitoring secretory membrane with FM1-43 fluorescence. *Annu Rev Neurosci* 22: 1-10, 1999.
15. **Federspil G, Baggio B, De PC, De CE, Borsatti A and Vettor R.** Effect of prolonged physical exercise on muscular phospholipase A2 activity in rats. *Diabete Metab* 13: 171-175, 1987.
16. **Gee KR, Brown KA, Chen WN, Bishop-Stewart J, Gray D and Johnson I.** Chemical and physiological characterization of fluo-4 Ca(2+)-indicator dyes. *Cell Calcium* 27: 97-106, 2000.
17. **Gissel H.** The role of Ca²⁺ in muscle cell damage. *Ann N Y Acad Sci* 1066: 166-180, 2005.

18. **Gutierrez JM and Ownby CL.** Skeletal muscle degeneration induced by venom phospholipases A2: insights into the mechanisms of local and systemic myotoxicity. *Toxicon* 42: 915-931, 2003.
19. **Harkins AB, Kurebayashi N and Baylor SM.** Resting myoplasmic free calcium in frog skeletal muscle fibers estimated with fluo-3. *Biophys J* 65: 865-881, 1993.
20. **Ho M, Post CM, Donahue LR, Lidov HG, Bronson RT, Goolsby H, Watkins SC, Cox GA and Brown RH, Jr.** Disruption of muscle membrane and phenotype divergence in two novel mouse models of dysferlin deficiency. *Hum Mol Genet* 13: 1999-2010, 2004.
21. **Hollingworth S, Zhao M and Baylor SM.** The amplitude and time course of the myoplasmic free [Ca²⁺] transient in fast-twitch fibers of mouse muscle. *J Gen Physiol* 108: 455-469, 1996.
22. **Idone V, Tam C, Goss JW, Toomre D, Pypaert M and Andrews NW.** Repair of injured plasma membrane by rapid Ca²⁺-dependent endocytosis. *J Cell Biol* 180: 905-914, 2008.
23. **Jobsis FF and Stainsby WN.** Oxidation of NADH during contractions of circulated mammalian skeletal muscle. *Respir Physiol* 4: 292-300, 1968.

24. **Klinge L, Laval S, Keers S, Haldane F, Straub V, Barresi R and Bushby K.**
From T-tubule to sarcolemma: damage-induced dysferlin translocation in early myogenesis. *FASEB J* 21: 1768-1776, 2007.
25. **Lennon NJ, Kho A, Bacskai BJ, Perlmutter SL, Hyman BT and Brown RH, Jr.**
Dysferlin interacts with annexins A1 and A2 and mediates sarcolemmal wound-healing. *J Biol Chem* 278: 50466-50473, 2003.
26. **Lieber RL, Woodburn TM and Friden J.** Muscle damage induced by eccentric contractions of 25% strain. *J Appl Physiol* 70: 2498-2507, 1991.
27. **McNeil PL and Khakee R.** Disruptions of muscle fiber plasma membranes. Role in exercise-induced damage. *Am J Pathol* 140: 1097-1109, 1992.
28. **McNeil PL and Kirchhausen T.** An emergency response team for membrane repair. *Nat Rev Mol Cell Biol* 6: 499-505, 2005.
29. **Mogil JS, Lichtensteiger CA and Wilson SG.** The effect of genotype on sensitivity to inflammatory nociception: characterization of resistant (A/J) and sensitive (C57BL/6J) inbred mouse strains. *Pain* 76: 115-125, 1998.

30. **Morgan DL, Claflin DR and Julian FJ.** The relationship between tension and slowly varying intracellular calcium concentration in intact frog skeletal muscle. *J Physiol* 500 (Pt 1): 177-192, 1997.
31. **Negulescu PA and Machen TE.** Intracellular ion activities and membrane transport in parietal cells measured with fluorescent dyes. *Methods Enzymol* 192: 38-81, 1990.
32. **Ng R, Metzger JM, Claflin DR and Faulkner JA.** Poloxamer 188 reduces the contraction-induced force decline in lumbrical muscles from *mdx* mice. *Am J Physiol Cell Physiol* 2008.
33. **Noakes TD.** Effect of exercise on serum enzyme activities in humans. *Sports Med* 4: 245-267, 1987.
34. **Petrof BJ, Shrager JB, Stedman HH, Kelly AM and Sweeney HL.** Dystrophin protects the sarcolemma from stresses developed during muscle contraction. *Proc Natl Acad Sci U S A* 90: 3710-3714, 1993.
35. **Street SF.** Lateral transmission of tension in frog myofibers: a myofibrillar network and transverse cytoskeletal connections are possible transmitters. *J Cell Physiol* 114: 346-364, 1983.

36. **Takekura H, Fujinami N, Nishizawa T, Ogasawara H and Kasuga N.** Eccentric exercise-induced morphological changes in the membrane systems involved in excitation-contraction coupling in rat skeletal muscle. *J Physiol* 533: 571-583, 2001.
37. **Tsien RY.** Fluorescent indicators of ion concentrations. *Methods Cell Biol* 30: 127-156, 1989.
38. **Warren GL, Hayes DA, Lowe DA and Armstrong RB.** Mechanical factors in the initiation of eccentric contraction-induced injury in rat soleus muscle. *J Physiol* 464: 457-475, 1993.
39. **Warren GL, Lowe DA, Hayes DA, Karwoski CJ, Prior BM and Armstrong RB.** Excitation failure in eccentric contraction-induced injury of mouse soleus muscle. *J Physiol* 468: 487-499, 1993.
40. **Williams DA, Head SI, Bakker AJ and Stephenson DG.** Resting calcium concentrations in isolated skeletal muscle fibres of dystrophic mice. *J Physiol* 428: 243-256, 1990.
41. **Wold LE, Dutta K, Mason MM, Ren J, Cala SE, Schwanke ML and Davidoff AJ.** Impaired SERCA function contributes to cardiomyocyte dysfunction in insulin resistant rats. *J Mol Cell Cardiol* 39: 297-307, 2005.

42. **Zuo L and Clanton TL.** Reactive oxygen species formation in the transition to hypoxia in skeletal muscle. *Am J Physiol Cell Physiol* 289: C207-C216, 2005.

Chapter 5

Summary and Conclusion

Overview

This overall purpose of this dissertation was to elucidate the contribution of membrane lesions to contraction-induced injuries in skeletal muscles. Prior to the research presented in this dissertation, the conditions that lead to the formation of sarcolemmal lesions were seldom characterized in an adequate manner. The lack of experimental data on contraction-induced sarcolemmal lesions was due in part to the limited number of skeletal muscle models that permitted lesions of membranes to be studied reliably. The techniques required for the study of membrane lesions, such as the use of fluorescence microscopy, membrane-staining dyes and large macromolecular compounds, could only be applied reliably to intact single muscle fiber preparations. On close scrutiny, we did not find the single muscle fiber preparation to be satisfactory model for the study of contraction-induced sarcolemmal lesions because the behavior of a single muscle fiber, existing without lateral connections to adjacent muscle fibers, was unlikely to represent accurately the function of single fibers in a whole muscle.

Accordingly, we developed a micro-sized whole muscle model utilizing the lumbrical muscle (LMB) from the forepaw of the mouse. The exceedingly small LMB muscle retains some of the diffusion benefits and visualization advantages normally

accorded to single muscle fiber preparations, while still maintaining a more accurate representation of *in vivo* whole muscle function. The remainder of this chapter will highlight the significant findings that arose from utilizing LMB muscles to study contraction-induced injury, as well as discuss the future direction of membrane-based muscle research.

LMB muscles as models to study contraction-induced injury (Chapter 2)

The goal of this study was to assess the potential of LMB muscles as models to study contractile activity. When subjected to 900 isometric contractions, LMB muscles remained viable throughout the 30 min contraction protocol and did not exhibit signs of fatigue or deterioration. This level of stability and robustness has never been demonstrated in any *in vitro* muscle preparation; conventional whole muscle models exhibit signs of fatigue even under less demanding contraction protocols (3). When subjected to an injurious protocol of repetitive lengthening contractions, LMB muscles showed signs of injury to individual fibers that could be visualized effectively and quantified by the use of appropriate dyes. The ability to visualize the injury in such detail immediately after a lengthening contraction protocol has never been achieved in an *in vitro* whole muscle preparation. Overall, LMB muscles were found to be (i) fluorescence-capable, (ii) sufficiently small to promote the diffusion of dyes and macromolecules (3), and (iii) stable even under severe metabolic demands. These features render the LMB muscle an attractive and reliable model to study contractile activity *in vitro*.

Membrane disruptions contribute to force deficits in dystrophic muscle (Chapter 3)

Using the LMB muscle preparation, we investigated the extent to which sarcolemmal disruptions contributed to the post-contraction force deficits of dystrophic mice. Application of a membrane-patching polymer (P188) and stretch-activated channel inhibitor reduced, almost completely, the contraction-induced force deficits of dystrophic muscles. These findings reinforced the direct relationship between sarcolemmal disruption and muscle dysfunction, and demonstrated that sarcolemmal lesions and stretch-activated ion channels accounted for almost the entire force deficit observed in dystrophic muscle. The results obtained in this study raised the prospect of developing therapeutic strategies directed at membrane stabilization of dystrophin-deficient skeletal muscle fibers.

No evidence of membrane lesions in wild-type muscle (Chapter 4)

Based on the positive findings from the previous chapter, we sought to determine if similar contraction-induced lesions also occurred in wild-type muscle. A novel fluorescence-based assay was developed, capable of detecting sarcolemmal breaches in real time. Utilizing this assay, we subjected wild-type LMB muscles to an acute protocol of severe lengthening contractions and did not find evidence of membrane lesions. Similar results were also obtained when the assay was applied to muscles that lacked dysferlin, a protein that is required for membrane repair (1). Taken together, these results suggested that sarcolemmal lesions were not contributory factors to the contraction-induced force deficits in wild-type muscle.

Conclusions and future research

The research presented in this dissertation has utilized a membrane-based approach to understand contraction-induced injuries. We demonstrate that sarcolemmal lesions play an important role in the contraction-induced force deficit of dystrophic muscle, but do not appear to be as significant in wild-type muscle. Future research should be directed at elucidating the contribution of other cellular events to contraction-induced injuries, such as the role of reactive oxygen species and proteolytic enzyme activity. Given the unique features of a micro-sized muscle preparation, these events should continue to be studied in the LMB muscle model. In addition, the LMB muscle offers an exciting prospect of examining whole muscle function from novel perspectives, such as those offered by ultra-sensitive fluorescence microscopy (5), RNA interference (4) and fluorescent protein techniques (2).

References

1. **Bansal D, Miyake K, Vogel SS, Groh S, Chen CC, Williamson R, McNeil PL and Campbell KP.** Defective membrane repair in dysferlin-deficient muscular dystrophy. *Nature* 423: 168-172, 2003.
2. **Muller-Taubenberger A and Anderson KI.** Recent advances using green and red fluorescent protein variants. *Appl Microbiol Biotechnol* 77: 1-12, 2007.
3. **Ng R, Metzger JM, Claffin DR and Faulkner JA.** Poloxamer 188 reduces the contraction-induced force decline in lumbrical muscles from *mdx* mice. *Am J Physiol Cell Physiol* 2008.
4. **Shrivastava N and Srivastava A.** RNA interference: an emerging generation of biologicals. *Biotechnol J* 3: 339-353, 2008.
5. **Zimmermann T, Rietdorf J and Pepperkok R.** Spectral imaging and its applications in live cell microscopy. *FEBS Lett* 546: 87-92, 2003.